J. Appl. Comput. Mech., 7(2) (2021) 671-700
DOI: 10.22055/JACM.2020.35439.2654

ISSN: 2383-4536
jacm.scu.ac.ir

Shahid Chamran University of Ahvaz

Journal of Applied and Computational Mechanics

Research Paper

A General Multibody Approach for the Linear and Nonlinear Stability Analysis of Bicycle Systems. Part II: Application to the Whipple-Carvallo Bicycle Model

Carmine Maria Pappalardo[1], Antonio Lettieri[2], Domenico Guida[3]

[1]Department of Industrial Engineering, University of Salerno, Via Giovanni Paolo II, 132, Fisciano, 84084, Salerno, Italy, Email: cpappalardo@unisa.it

[2]Spin-Off MEID4 s.r.l., University of Salerno, Via Giovanni Paolo II, 132, Fisciano, 84084, Salerno, Italy, Email: a.lettieri20@gmail.com

[3]Department of Industrial Engineering, University of Salerno, Via Giovanni Paolo II, 132, Fisciano, 84084, Salerno, Italy, Email: guida@unisa.it

Received October 14 2020; Revised November 30 2020; Accepted for publication November 30 2020.
Corresponding author: Carmine Maria Pappalardo (cpappalardo@unisa.it)

Abstract. This paper represents the second contribution of a two-part research work presenting the application of the proposed multibody analysis approach to bicycle systems and the relative numerical results found. In this work, a nonlinear multibody model of a bicycle system is developed and implemented to perform a parametric analysis to understand the influence of the variation of the principal model parameters on the system stability under investigation. To demonstrate the effectiveness of the proposed approach, the case study considered in this paper is the dynamic analysis of the Whipple-Carvallo bicycle model. Considering the combined use of a robust numerical technique for nonlinear dynamical simulations with a specifically devised linearization procedure, the effects of the different geometric parameters and inertial properties on the bicycle stability are investigated. The numerical results obtained in this work using the proposed multibody techniques are useful to gain insight information about the dynamic behavior of the bicycle system in a straight motion. The proposed multibody methodology also demonstrated a high potential for analyzing complex multibody mechanical systems in virtue of the generality of the analytical and computational approaches adopted.

Keywords: Multibody System Dynamics, Stability Analysis, Parametric Study, Whipple-Carvallo Bicycle Model.

1. Introduction

In this section, an introduction to the topics of interest for this paper is provided. To this end, some background material is reported for clarifying the collocation of the current research work. Subsequently, a short literature review of the dynamics of two-wheeled vehicles is given. Then, the scope and the contributions of this investigation are discussed, followed by the organization of the paper.

1.1 Background and Significance of the Present Research Work

This paper deals with the multibody analysis of the Whipple-Carvallo bicycle model [1–5]. In general, a large variety of mechanical systems can be analyzed to investigate their dynamical behavior within the multibody computational framework using a systematic computational procedure based on sound analytical grounds [6–8]. In particular, the development of the multibody system dynamics significantly changed the approach to vehicle modeling and the optimization of their performance [9–11]. Road vehicles, and rail vehicles, can be readily described employing the multibody approach since their dynamic behavior is strongly influenced by the formulation of the contact forces that describe the interaction with the ground or with the rail [12–14]. Besides, in addition to typical mechanical systems such as vehicles and robots [15, 16], biomechanical systems can also be modeled using the multibody approach to the dynamics of articulated systems [17–19]. On the other hand, in the case of two-wheeled vehicles, which represent the focus of the current investigation, the design of the system geometric parameters plays a central role. In contrast, the influence of the rider is of fundamental importance in their dynamics, and there are many strategies to model the overall system behavior [20, 21]. Therefore, this paper is collocated in the framework of the dynamic analysis of mechanical systems based on the multibody approach and is specifically focused on the mechanical analysis of the bicycle system.

1.2 Literature Review on Two-Wheeled Vehicles

Bicycles can be modeled in several ways, such as multibody systems, and, despite their apparent simplicity, their dynamical behavior is fascinating. The pioneering significant contributions to the study of the bicycle dynamics are the works of Whipple [22] and Carvallo [23], who were the first to derive the nonlinear equations of motion of bicycle systems, as testified in the literature [24–27]. All subsequent works usually start from the models of Whipple and Carvallo, and many authors, such as Papadopoulos [28], Meijaard [29], and Schwab et al. [30], verified the equations found by Whipple and employed them to validate their models. In this direction, Meijaard et al. proposed in [4] a benchmark model of the Whipple-Carvallo bicycle system, which can be used to validate other models obtained with different analytical approaches. Since the equations of motion of the bicycle assume a complex form,

the dynamic model of the bicycle system proposed by Meijaard et al. can be used as a benchmark for the validation of other models [4]. Other interesting works, which try to summarize the different mathematical models, analysis methods, and numerical results, with an overview also on the control problem, are the papers of Kooijman and Schwab [31], Limebeer and Sharp [32], and Schwab and Meijaard [33].

In the scientific literature concerning the dynamics of bicycle and two-wheeled systems in general, the most studied phenomenon is undoubtedly the self-stability of the vehicle, which was analyzed with several interesting analytical techniques by a large number of authors. For instance, Xiong et al. analyzed the stability of the bicycle using the center manifold theorem. They derived the equation of motion with the use of the Gibbs-Appell method to analyze the system stability [34]. Simultaneously, in [35], the same research group carried out the stability study of the circular motion of the bicycle collocated on a revolution surface. Their numerical results are in agreement with the work done by Basu-Mandal et al. in [36], who validated the model proposed by them using the benchmark bicycle model. The bicycle model also suits educational purposes, as pointed out by Escalona and Recuero in [37], who used the Whipple-Carvallo bicycle system to teach the basics of the multibody approach to the analysis of constrained mechanical systems.

The Whipple-Carvallo model is the simplest dynamical model of a bicycle that exhibits the well-known auto-stability behavior during a straight motion, which fundamentally depends on the geometry of the bicycle [25–27]. To demonstrate this aspect, experimental validations and comparison with real instrumented bicycles can be found in the work of Kooijman et al. [5] and Escalona et al. [38]. Starting from the Whipple-Carvallo bicycle model, different simplifying hypotheses can be relaxed to improve the accuracy of the virtual simulations. For example, in the case of the use of toroidal wheels shown in the work of Frosali and Ricci [39], and Astrom et al. [40]. Also, including more degrees of freedom that lead to more complex models allows for gaining more information on the dynamic behavior of the bicycle. For this purpose, Ploch et al. in [41] included a tire model, a passive rider, and the flexibility of the frame to address the instability resulting from the wobble motion, which is associated with an unstable vibration of the steering system and cannot be studied using the Whipple-Carvallo bicycle model. A more complex study of this phenomenon can be found in the work of Tomiati et al. [42], where a nonlinear tire model is included to study the nonlinear wobble instability. On the other hand, more accurate modeling of the rider can help understand the importance of its role to control and stabilize the rider-bicycle system, as shown by Schwab et al. in their work [43], where the effects of the posture of the rider are taken into account. Furthermore, the rider modeling can also be used to study the performances of athletes, as showed by Jansen and McPhee in [44]. More accurate hypotheses concerning two-wheeled vehicles in general, such as the tire-road forces, the frame compliance, and the presence of front and rear suspension systems, are usually used to develop models of motorcycles. The excellent book of Cossalter gives a complete overview of the modeling issues and the corresponding solution strategies related to these problems [24]. An insight into the development of multibody models can also be seen in the works of Cossalter et al. [45, 46], where different analyses and considerations on the suspension system schemes are provided. Other significant information and developments can be found in the interesting work of Sharp et al. [47], where different engineering aspects such as the tire-road contact, the geometry and force modeling, the design of suspension schemes, and also the analysis of steering control systems are considered [48, 49].

1.3 Scope and Contribution of this Study

In this paper, the focus is on analyzing a bicycle model where the pure rolling conditions of the wheels are applied as a set of nonholonomic constraints, as will be explained in detail below in the manuscript. In general, nonholonomic systems have a peculiar property, which consists of the possibility of exhibiting asymptotic stability even though there is no explicit formulation of energy dissipation in the model. Several authors studied this behavior through the years like, for example, Zenkov et al. in [50], and Ruina in [51]. One of the most studied examples of nonholonomic mechanical systems that show this unique property is the Chaplygin sleigh model [52, 53]. This dynamical system is often taken as a reference since, despite its simplicity, its dynamical characteristics can also be found in more complex nonlinear nonholonomic systems, such as the swimming robot studied by Pollard et al. in [54]. The use of nonholonomic constraints can be quite interesting when the interaction between the system of interest and the external environment must be modeled, as in the case of the development of general control strategies [55–57]. This is also the case when modeling the contact between the bicycle wheels and the ground through appropriate nonholonomic constraints, like those considered in the bicycle model of interest for this investigation. However, as discussed above in the literature survey about the dynamics of bicycle systems, it is difficult to find a systematic approach for the analytical formulation of the differential-algebraic equations of motion of bicycle systems consistent with a fully Lagrangian approach featuring holonomic and nonholonomic constraints. Similarly, a straightforward method for linearizing the constrained dynamical model to carry out the stability analysis and a robust numerical procedure for the computer simulations of both linear and nonlinear bicycle models cannot be found in the literature as well. Therefore, this paper proposes an analytical approach and a computational procedure to fill these gaps.

In this work, one of the main goals is to demonstrate the advantages of using the alternative analytical methodology proposed in this two-part investigation to linearize the nonlinear equations of motion of a general class of multibody mechanical systems. The family of multibody systems of interest for this paper is general and encompasses holonomic and nonholonomic systems whose dynamic equations are obtained within a general multibody formulation framework by using the D'Alambert-Lagrange principle of virtual work and the technique of the Lagrange multipliers. As shown in the manuscript, by directly considering the index-three set of differential-algebraic equations of motion describing the model of the multibody system of interest, namely the Whipple-Carvallo bicycle model, one can systematically linearize the dynamic model for performing the stability analysis based on a modal decomposition method considering a computer-aided approach based on a mixed symbolic-numeric computation paradigm. By doing so, a multibody model of the Whipple-Carvallo bicycle system is constructed at first. Subsequently, the nonlinear differential-algebraic equations of motion of the bicycle system are fully and systematically linearized. Finally, a general-purpose multibody code for the dynamic analysis of two-wheeled systems is readily developed to create a virtual environment for performing numerical simulations. Besides, the numerical results obtained from the stability analysis compared to the benchmark bicycle models are readily verified. To this end, a robust multibody computational algorithm for handling holonomic and nonholonomic multibody systems is developed in the first part of this two-part paper, and its use is demonstrated in the second part of this two-part paper considering the proposed mechanical model of the Whipple-Carvallo bicycle system.

The computational hurdles in obtaining a multibody algorithm that is general, robust, effective, efficient, and relatively easy to be implemented in a numerical code are highlighted by several interesting studies and viable approaches analyzed through the years [58–61]. Thus, to address this fundamental issue in this two-part investigation, the combined use of appropriate modifications in the generalized partitioning method and the augmented Lagrangian formulation of the equation of motion for the dynamic analysis of constrained multibody systems led in the first paper to the formulation of the so-called Robust Generalized Coordinate Partitioning Algorithm (RGCPA). This second paper presents the advantages of the proposed computational method and the possibilities of application to general multibody mechanical systems also in the presence of nonholonomic constraints. The proposed approach, which is applied to the analysis of the multibody model of the Whipple-Carvallo bicycle system developed in this paper, results in being well suited for computer implementation and significantly improves the quality of the numerical solution found for the problem interest.

In summary, the main scope and the fundamental contributions of the present paper can be synthesized, as reported below.

(1) The paper proposes a general multibody model of the Whipple-Carvallo bicycle system, which can also be readily modified and adapted to represent bicycle models that substantially differ from those found in the literature. The bicycle model developed in this work is completely nonlinear and nonholonomic. It is structured following a general parametric approach, ranging from the bicycle geometry to its inertial properties, and allows for performing a systematic parametric analysis of the bicycle stability. Using the analytical methods and the computational procedures developed in the paper, the nonlinear stability of the Whipple-Carvallo bicycle system is studied. Its linear dynamical behavior is evaluated by drawing a stability map representing the typical weave, capsize, and castering eigenmodes.

(2) To verify the correctness and reliability of the numerical results obtained through the computer simulations developed in this investigation, the linearized version of the multibody model of the bicycle system devised in the paper is compared first with the benchmark models of the Whipple-Carvallo bicycle system found in the literature, namely, by assuming as references two different bicycle models, with and without the presence of the rider. Subsequently, a stability influence index is proposed and used to carry out a thorough parametric study for identifying the subset of geometry and inertial model parameters that have the highest impact on the stability of the bicycle system. Finally, the interesting model parameters are isolated, and their effects on bicycle stability are separately investigated one by one.

(3) The last part of this investigation is focused on the stability analysis of the nonlinear multibody model of the Whipple-Carvallo bicycle system considering small perturbations of the numerical values of the most relevant model parameters that were identified from the parametric study. The analytical methodologies and the computational procedures developed in this work played a central role in achieving this goal. For this purpose, several numerical simulations were used as demonstrative examples of the stabilizing influence of the relevant model parameters by varying them in reasonable ranges.

To evaluate the reliability of the proposed methods from the numerical experiments carried out in the second part of this investigation composed of two parts, an excellent agreement was found in the comparison of the proposed multibody model of the Whipple-Carvallo bicycle system with the reference benchmark models, thereby demonstrating the effectiveness of the analytical and computational approaches devised in this paper.

1.4 Organization of the Manuscript

The remaining sections of this research paper are organized as follows. In Section 2., the multibody model of the Whipple-Carvallo bicycle system developed by the authors in this investigation is explained in detail. In Section 3., the numerical results obtained from the stability analysis of the straight motion of the bicycle multibody model are reported, a comparative analysis between the proposed nonlinear model and the linear benchmark models found in the literature is discussed, and a parametric analysis focused on the principal features that influence the bicycle stability is presented. Section 4. provides a summary of the paper, the conclusions of this research work, and some interesting topics that could be promising as future research directions starting from the final results obtained in this investigation.

2. Bicycle Multibody Model

In this section, the multibody model of the Whipple-Carvallo bicycle system developed in the paper is described in detail.

2.1 Kinematic Model

In this subsection, the description of the kinematic model of the bicycle system is reported. The schematic representation of the bicycle multibody model considered in this work is shown in Figure 1.

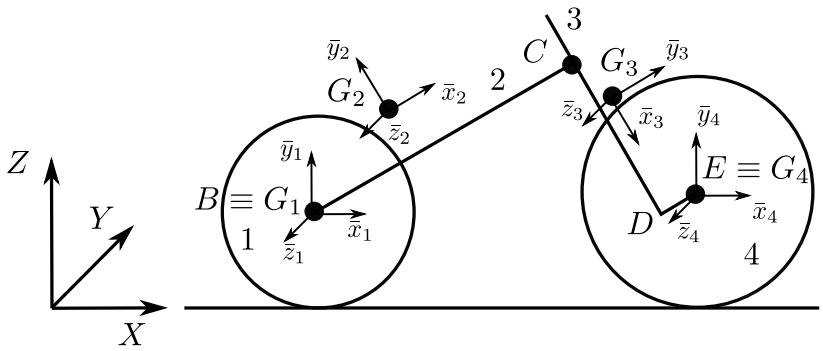

Figure 1. *Bicycle multibody model.*

As shown in Figure 1, the multibody model of the Whipple-Carvallo bicycle system is composed of four rigid bodies and, therefore, $N_b = 4$. From the first to the fourth, the bodies that form the mechanical model of the bicycle system are the rear wheel (body 1), the rear frame (body 2), the front frame (body 3), and the front wheel (body 4). For simplicity, the rear frame includes the rider modeled as a rigid body attached to it. The kinematics of each rigid body is described using a set of six generalized coordinates, grouped in the configuration vector denoted with $\boldsymbol{q}_i$ having dimension $n_r = 6$, which includes three translational coordinates, grouped in the position vector $\boldsymbol{R}_i$, and three rotational coordinates, grouped in the orientation vector $\boldsymbol{\theta}_i$, where the subscript i indicates the integer number labeling the generic rigid body. Thus, the generalized coordinates vector of each body can be written as:

$$\boldsymbol{q}_i = \begin{bmatrix} \boldsymbol{R}_i \\ \boldsymbol{\theta}_i \end{bmatrix} \tag{1}$$

where:

$$\boldsymbol{R}_i = \begin{bmatrix} x_i & y_i & z_i \end{bmatrix}^T, \quad \boldsymbol{\theta}_i = \begin{bmatrix} \phi_i & \vartheta_i & \psi_i \end{bmatrix}^T \tag{2}$$

where the integer number that labels the rigid bodies is $i = 1, ..., 4$, while x_i, y_i, and z_i respectively represent the longitudinal, lateral, and vertical displacements of the center of mass of the generic body i, whereas ϕ_i, ϑ_i, and ψ_i respectively indicate the roll, yaw, and pitch angular displacements of the generic body i. The set of rotational coordinates employed for describing the orientation of the frame of reference attached to each rigid body is the set of Tait-Bryan angles, that is, the set of Euler angles based on the X-Y-Z sequence. Therefore, the rotation matrix of the generic rigid body i denoted with $\boldsymbol{A}_i$ can be written as three subsequent rotations around the three axes of the local reference systems respectively indicated with $\bar{x}_i$, $\bar{y}_i$, and $\bar{z}_i$ as follows:

$$\boldsymbol{A}_i = \boldsymbol{A}_{\bar{x}_i} \boldsymbol{A}_{\bar{y}_i} \boldsymbol{A}_{\bar{z}_i} \tag{3}$$

where:

$$\boldsymbol{A}_{\bar{x}_i} = \begin{bmatrix} 1 & 0 & 0 \\ 0 & \cos(\phi_i) & -\sin(\phi_i) \\ 0 & \sin(\phi_i) & \cos(\phi_i) \end{bmatrix}, \quad \boldsymbol{A}_{\bar{y}_i} = \begin{bmatrix} \cos(\vartheta_i) & 0 & \sin(\vartheta_i) \\ 0 & 1 & 0 \\ -\sin(\vartheta_i) & 0 & \cos(\vartheta_i) \end{bmatrix} \tag{4}$$

and

$$\boldsymbol{A}_{\bar{z}_i} = \begin{bmatrix} \cos(\psi_i) & -\sin(\psi_i) & 0 \\ \sin(\psi_i) & \cos(\psi_i) & 0 \\ 0 & 0 & 1 \end{bmatrix} \tag{5}$$

Before performing the sequential rotations that define the final orientation of each body-fixed reference system with respect to the global reference system, the local reference systems of each body of the bicycle multibody model are initially oriented in the space to be parallel to the inertial reference frame employed as the global reference system. Thus, since the bicycle system is composed only of rigid bodies, the kinematics of this multibody system can be readily defined by using the fundamental equations of rigid kinematics given by:

$$\begin{cases} \boldsymbol{r}_i(P) = \boldsymbol{R}_i + \boldsymbol{A}_i \bar{\boldsymbol{u}}_i(P) \\ \\ \boldsymbol{v}_i(P) = \dot{\boldsymbol{R}}_i + \boldsymbol{A}_i \left(\bar{\boldsymbol{\omega}}_i \times \bar{\boldsymbol{u}}_i(P) \right) \\ \\ \boldsymbol{a}_i(P) = \ddot{\boldsymbol{R}}_i + \boldsymbol{A}_i \left(\dot{\bar{\boldsymbol{\omega}}}_i \times \bar{\boldsymbol{u}}_i(P) \right) + \boldsymbol{A}_i \left(\bar{\boldsymbol{\omega}}_i \times \left(\bar{\boldsymbol{\omega}}_i \times \bar{\boldsymbol{u}}_i(P) \right) \right) \end{cases} \tag{6}$$

where the global vectors $\boldsymbol{r}_i(P)$, $\boldsymbol{v}_i(P)$, and $\boldsymbol{a}_i(P)$ respectively represent the position, velocity, and acceleration vectors of the generic point P collocated on the rigid body i, $\bar{\boldsymbol{u}}_i(P)$ is the local position vector of the point P of the rigid body i, while $\bar{\boldsymbol{\omega}}_i$ denotes the local angular velocity vector of the rigid body i. The local angular velocity vector $\bar{\boldsymbol{\omega}}_i$ can be written as a linear combination of the time derivatives of the rotational coordinates included in the vector $\dot{\boldsymbol{\theta}}_i$ as follows:

$$\bar{\boldsymbol{\omega}}_i = \bar{\boldsymbol{G}}_i \dot{\boldsymbol{\theta}}_i \tag{7}$$

where the transformation matrix denoted with $\bar{\boldsymbol{G}}_i$ is associated with the X-Y-Z sequence of Euler angles and is defined as:

$$\bar{\boldsymbol{G}}_i = \begin{bmatrix} \cos(\theta_i)\cos(\psi_i) & \sin(\psi_i) & 0 \\ -\cos(\theta_i)\sin(\psi_i) & \cos(\psi_i) & 0 \\ \sin(\theta_i) & 0 & 1 \end{bmatrix} \tag{8}$$

Similarly, it can be easily proved that the velocity and acceleration vectors $\boldsymbol{v}_i(P)$ and $\boldsymbol{a}_i(P)$ associated with a generic material point P of the rigid body i can be written as linear combinations of the generalized velocity and acceleration vectors $\dot{\boldsymbol{q}}_i$ and $\ddot{\boldsymbol{q}}_i$ as follows:

$$\begin{cases} \boldsymbol{v}_i(P) = \boldsymbol{L}_i(P) \dot{\boldsymbol{q}}_i \\ \\ \boldsymbol{a}_i(P) = \boldsymbol{L}_i(P) \ddot{\boldsymbol{q}}_i + \dot{\boldsymbol{L}}_i(P) \dot{\boldsymbol{q}}_i \end{cases} \tag{9}$$

where the matrix $\boldsymbol{L}_i(P)$ represents the Jacobian matrix of the position vector $\boldsymbol{r}_i(P)$ of the generic point P of the rigid body i evaluated with respect to the generalized coordinate vector $\boldsymbol{q}_i$ of the rigid body i. This fundamental matrix is defined as a block matrix as follows:

$$\boldsymbol{L}_i(P) = \frac{\partial \boldsymbol{r}_i(P)}{\partial \boldsymbol{q}_i} = \begin{bmatrix} \boldsymbol{L}_{R_i}(P) & \boldsymbol{L}_{\theta_i}(P) \end{bmatrix} = \begin{bmatrix} \boldsymbol{I} & \boldsymbol{A}_i \tilde{\bar{\boldsymbol{u}}}_i^T(P) \bar{\boldsymbol{G}}_i \end{bmatrix} \tag{10}$$

where $\tilde{\bar{\boldsymbol{u}}}_i(P)$ is the skew-symmetric matrix used for defining the cross product with its axial vector $\bar{\boldsymbol{u}}_i(P)$. It is, therefore, apparent that the definition of the kinematic model of multibody system under consideration requires the knowledge of the system configuration vector $\boldsymbol{q}_i$ and its time derivatives $\dot{\boldsymbol{q}}_i$ and $\ddot{\boldsymbol{q}}_i$.

2.2 Geometric Parameters

In this subsection, the definition of the fundamental geometric parameters employed for describing the bicycle system is presented. The geometric parameters and the fundamental quantities that serve to describe the kinematic chain of the multibody model are represented in Figure 2.

To simplify the geometric construction of the bicycle mechanical model, the following parametric description for the model geometry is devised in this paper. First, six parameters are identified as the set of independent quantities employed for the geometric description of the bicycle system. Subsequently, an analytic approach based on a geometric construction of a kinematic chain is used to describe in a parametric fashion the reference points that serve to define the geometric configuration of the bicycle system univocally. Thus, the set of six independent geometric parameters considered herein can be seen as the set of geometric degrees of freedom of the bicycle multibody model. The definition of the parameters contained in this set serves to identify the geometry of the model under consideration completely. The six independent geometric quantities assumed as independent parameters that are used for the description of the bicycle model are the rear wheel radius denoted with R_r, the front wheel radius denoted with R_f, the bicycle wheelbase denoted with W_b, the fork offset denoted with H_f, the rear frame angle denoted with β, and the caster

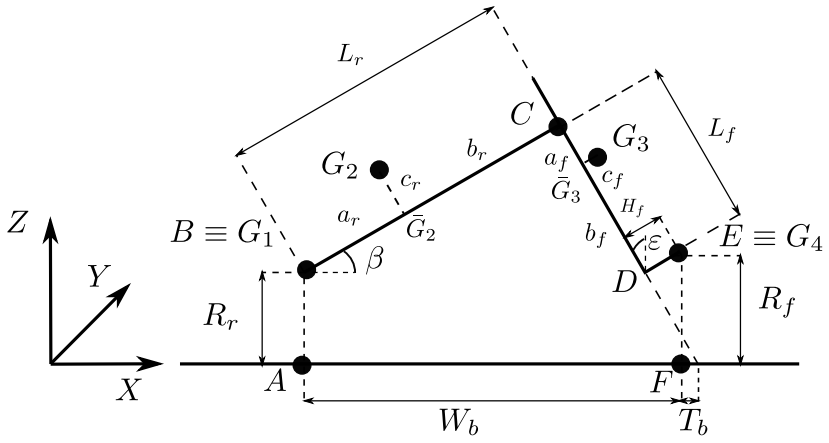

Figure 2. *Bicycle geometric parameters.*

angle denoted with ε. For simplicity, the independent geometric parameters useful for the representation of the bicycle geometric model are grouped in the parameter vector indicated with $\boldsymbol{b}_g$ and defined as:

$$\boldsymbol{b}_g = \begin{bmatrix} R_r & R_f & W_b & H_f & \beta & \varepsilon \end{bmatrix}^T \tag{11}$$

where the vector of geometric parameters $\boldsymbol{b}_g$ is formed by $n_{b,g} = 6$ parameters. On the other hand, the geometric points assumed as reference points for constructing the kinematic chain associated with the bicycle multibody model are the points A, B, C, D, E, and F of Figure 2. Thus, one can write the global positions of the set of bicycle references points in terms of the set of independent geometric parameters by using a kinematic chain approach as follows:

$$\begin{cases} \boldsymbol{r}_A = \begin{bmatrix} 0 \\ 0 \\ 0 \end{bmatrix}, \quad \boldsymbol{r}_B = \boldsymbol{r}_A + \begin{bmatrix} 0 \\ 0 \\ R_r \end{bmatrix} \\ \boldsymbol{r}_C = \boldsymbol{r}_B + \begin{bmatrix} L_r \cos(\beta) \\ 0 \\ L_r \sin(\beta) \end{bmatrix}, \quad \boldsymbol{r}_D = \boldsymbol{r}_C + \begin{bmatrix} L_f \cos(\varepsilon + \frac{3}{2}\pi) \\ 0 \\ L_f \sin(\varepsilon + \frac{3}{2}\pi) \end{bmatrix} \\ \boldsymbol{r}_E = \boldsymbol{r}_D + \begin{bmatrix} H_f \cos(\varepsilon) \\ 0 \\ H_f \sin(\varepsilon) \end{bmatrix}, \quad \boldsymbol{r}_F = \boldsymbol{r}_E + \begin{bmatrix} 0 \\ -R_f \\ 0 \end{bmatrix} = \begin{bmatrix} W_b \\ 0 \\ 0 \end{bmatrix} \end{cases} \tag{12}$$

where the geometric parameter denoted with L_r represents the length of the rear frame, while the geometric parameter denoted with L_f represents the length of the front frame. These two geometric quantities can be readily calculated in terms of the set of independent geometric parameters as follows:

$$\begin{cases} L_r = \frac{\cos(\varepsilon)\left(W_b - H_f\cos(\varepsilon)\right) + \sin(\varepsilon)\left(R_f - R_r - H_f\sin(\varepsilon)\right)}{\cos(\beta - \varepsilon)} \\ L_f = \frac{\sin(\beta)\left(W_b - H_f\cos(\varepsilon)\right) - \cos(\beta)\left(R_f - R_r - H_f\sin(\varepsilon)\right)}{\cos(\beta - \varepsilon)} \end{cases} \tag{13}$$

Another important geometric parameter relevant in the description of the bicycle multibody model is the bicycle geometric trail that is denoted with T_b. This geometric quantity can be obtained as a function of the six independent geometric parameters chosen to describe the bicycle model as follows:

$$T_b = R_f \tan(\varepsilon) - \frac{H_f}{\cos(\varepsilon)} \tag{14}$$

Even though the geometric trail is not essential to describe the bicycle geometric model using the kinematic chain construction and the design approach employed in this paper, this parameter represents an important geometric feature that can provide significant information on the dynamic behavior of the Whipple-Carvallo bicycle system.

As discussed above, by using the modeling approach proposed in this paper, the mechanical model of the Whipple-Carvallo bicycle system can be fully described by using Equations (12), (13), and (14), which are written in terms of the geometric information contained in the vector of independent geometric parameters. In fact, all the geometric parameters necessary for identifying the configurations of the rigid bodies and the collocations of the mechanical joints of the multibody model can be readily obtained in terms of the six independent geometric parameters defined in the paper. To this end, the next step necessary for the description of the bicycle mechanical model and the identification of the kinematic pairs that form the mechanical joints is represented by the geometric determination of the initial configuration of the multibody system. The bicycle initial configuration is described using the global position vectors of the centers of mass of the four bodies of the model and the corresponding rotational coordinate vectors that describe the relative orientation between the body-fixed coordinate systems and the global frame of reference. In particular, as mentioned before, the global position vectors of the centers of mass of the bicycle rigid bodies are indicated as $\boldsymbol{R}_i$, while the rotational coordinate vectors associated to each rigid body are indicated with $\boldsymbol{\theta}_i$, where $i = 1, ..., 4$ refers to the four bodies of the model. For the bicycle multibody model developed in this work, these vector quantities are reported in Table 1.

Table 1. Generalized coordinates and generalized velocities of the four bodies of the bicycle multibody model.

Coordinate vectors	Body 1	Body 2	Body 3	Body 4
$\boldsymbol{R}_i$	$\begin{bmatrix} 0 \\ 0 \\ R_r \end{bmatrix}$	$\begin{bmatrix} a_r \cos(\beta) + c_r \cos(\beta + \frac{\pi}{2}) \\ 0 \\ a_r \sin(\beta) + c_r \sin(\beta + \frac{\pi}{2}) \end{bmatrix}$	$\begin{bmatrix} L_r \cos(\beta) + a_f \cos(\varepsilon + \frac{3}{2}\pi) + c_f \cos(\varepsilon) \\ 0 \\ L_r \sin(\beta) + a_f \sin(\varepsilon + \frac{3}{2}\pi) + c_f \sin(\varepsilon) \end{bmatrix}$	$\begin{bmatrix} L_r \cos(\beta) + L_f \cos(\varepsilon + \frac{3}{2}\pi) + H_f \cos(\varepsilon) \\ 0 \\ L_r \sin(\beta) + L_f \sin(\varepsilon + \frac{3}{2}\pi) + H_f \sin(\varepsilon) \end{bmatrix}$
$\boldsymbol{\theta}_i$	$\begin{bmatrix} \frac{\pi}{2} \\ 0 \\ 0 \end{bmatrix}$	$\begin{bmatrix} \frac{\pi}{2} \\ 0 \\ \beta \end{bmatrix}$	$\begin{bmatrix} \frac{\pi}{2} \\ 0 \\ \varepsilon + \frac{3}{2}\pi \end{bmatrix}$	$\begin{bmatrix} \frac{\pi}{2} \\ 0 \\ 0 \end{bmatrix}$
$\boldsymbol{q}_i$	$\begin{bmatrix} \boldsymbol{R}_1 \\ \boldsymbol{\theta}_1 \end{bmatrix}$	$\begin{bmatrix} \boldsymbol{R}_2 \\ \boldsymbol{\theta}_2 \end{bmatrix}$	$\begin{bmatrix} \boldsymbol{R}_3 \\ \boldsymbol{\theta}_3 \end{bmatrix}$	$\begin{bmatrix} \boldsymbol{R}_4 \\ \boldsymbol{\theta}_4 \end{bmatrix}$
$\dot{\boldsymbol{R}}_i$	$\begin{bmatrix} -\omega R_r \\ 0 \\ 0 \end{bmatrix}$	$\begin{bmatrix} -\omega R_r \\ 0 \\ 0 \end{bmatrix}$	$\begin{bmatrix} -\omega R_r \\ 0 \\ 0 \end{bmatrix}$	$\begin{bmatrix} -\omega R_r \\ 0 \\ 0 \end{bmatrix}$
$\dot{\boldsymbol{\theta}}_i$	$\begin{bmatrix} 0 \\ 0 \\ \omega \end{bmatrix}$	$\begin{bmatrix} 0 \\ 0 \\ 0 \end{bmatrix}$	$\begin{bmatrix} 0 \\ 0 \\ 0 \end{bmatrix}$	$\begin{bmatrix} 0 \\ 0 \\ \omega \left(R_r / R_f\right) \end{bmatrix}$
$\dot{\boldsymbol{q}}_i$	$\begin{bmatrix} \dot{\boldsymbol{R}}_1 \\ \dot{\boldsymbol{\theta}}_1 \end{bmatrix}$	$\begin{bmatrix} \dot{\boldsymbol{R}}_2 \\ \dot{\boldsymbol{\theta}}_2 \end{bmatrix}$	$\begin{bmatrix} \dot{\boldsymbol{R}}_3 \\ \dot{\boldsymbol{\theta}}_3 \end{bmatrix}$	$\begin{bmatrix} \dot{\boldsymbol{R}}_4 \\ \dot{\boldsymbol{\theta}}_4 \end{bmatrix}$

In order to achieve this goal, in this paper the geometric distances respectively denoted with a_r, a_f, b_r, b_f, c_r, and c_f, which are respectively represented in Figure 2, are introduced and used to simplify the geometric description of the bicycle multibody model. While the geometric distances a_r, b_r, and c_r refer to rear frame, the geometric distances a_f, b_f, and c_f are associated with the front frame. The introduction of this additional set of geometric parameters has a threefold purpose. First, they are employed to facilitate identifying the collocations of the centers of mass of both the rear and front frames. Second, they serve to easily include in the present multibody model the geometric information coming from the benchmark model of the Whipple-Carvallo bicycle system available in the literature. Third, they allow for performing a systematic parametric analysis of the dynamic behavior of the bicycle multibody model developed in this work in the case of both linear and nonlinear dynamical scenarios. Starting from the absolute position vector of the rear frame center of mass known from the benchmark model of the Whipple-Carvallo bicycle system, the geometric distances relative to the rear frame indicated with a_r and b_r can be respectively calculated as:

$$\begin{cases} a_r = (\boldsymbol{R}_2 - \boldsymbol{r}_B)^T \boldsymbol{s}_{B,C} \\ b_r = (\boldsymbol{r}_C - \boldsymbol{R}_2)^T \boldsymbol{s}_{B,C} \end{cases}, \quad \boldsymbol{s}_{B,C} = \frac{\boldsymbol{r}_C - \boldsymbol{r}_B}{\|\boldsymbol{r}_C - \boldsymbol{r}_B\|} \tag{15}$$

where the geometric vector denoted with $\boldsymbol{s}_{B,C}$ is the unit vector that indicates the direction of the line passing through the points B and C collocated on the rear frame. The last geometric distance relative to the rear frame indicated with c_r can be computed as:

$$c_r = \left\| \boldsymbol{R}_2 - \boldsymbol{r}_{\bar{G}_2} \right\|, \quad \boldsymbol{r}_{\bar{G}_2} = \boldsymbol{r}_B + a_r \boldsymbol{s}_{B,C} \tag{16}$$

where the geometric vector denoted with $\boldsymbol{r}_{\bar{G}_2}$ is the global position vector of the point $\bar{G}_2$ resulting from the projection of the rear frame center of mass indicated with G_2 on the line that represents the rear frame. By using the same approach for performing the geometric construction, the geometric distances relative to the front frame indicated with a_f and b_f can be respectively calculated as:

$$\begin{cases} a_f = (\boldsymbol{R}_3 - \boldsymbol{r}_C)^T \boldsymbol{s}_{C,D} \\ b_f = (\boldsymbol{r}_D - \boldsymbol{R}_3)^T \boldsymbol{s}_{C,D} \end{cases}, \quad \boldsymbol{s}_{C,D} = \frac{\boldsymbol{r}_D - \boldsymbol{r}_C}{\|\boldsymbol{r}_D - \boldsymbol{r}_C\|} \tag{17}$$

where the geometric vector denoted with $\boldsymbol{s}_{C,D}$ is the unit vector that indicates the direction of the line passing through the points C and D collocated on the front frame. The last geometric distance relative to the front frame indicated with c_f can be computed as:

$$c_f = \left\| \boldsymbol{R}_3 - \boldsymbol{r}_{\bar{G}_3} \right\|, \quad \boldsymbol{r}_{\bar{G}_3} = \boldsymbol{r}_C + a_f \boldsymbol{s}_{C,D} \tag{18}$$

where the geometric vector denoted with $\boldsymbol{r}_{\bar{G}_3}$ is the global position vector of the point $\bar{G}_3$ resulting from the projection of the front frame center of mass indicated with G_3 on the line that represents the front frame. The definition of the previous additional set of geometric distances concludes the description of the bicycle multibody model in terms of its fundamental geometric parameters.

2.3 Dynamic Model

In this subsection, the nonlinear equations of motion that govern the dynamic behavior of the bicycle system are derived. To this end, a Lagrangian approach is employed in conjunction with the basic principles of analytical mechanics [62,63]. For simplicity, the kinetic energy of the generic rigid body i is denoted with T_i, while the potential energy for the same body is indicated with U_i. The following general formulations respectively give these scalar quantities:

$$T_i = \frac{1}{2} m_i \dot{\boldsymbol{R}}_i^T \dot{\boldsymbol{R}}_i + \frac{1}{2} \bar{\boldsymbol{\omega}}_i^T \bar{\boldsymbol{I}}_{G_i} \bar{\boldsymbol{\omega}}_i + m_i \dot{\boldsymbol{R}}_i^T \boldsymbol{A}_i \tilde{\bar{\boldsymbol{u}}}_i^T(G_i) \bar{\boldsymbol{\omega}}_i \tag{19}$$

and

$$U_i = m_i g z_i \tag{20}$$

where g is the gravity acceleration, $\bar{\boldsymbol{u}}_i(G_i)$ indicates the local position vector of the center of mass G_i relative to the generic body i, $\tilde{\bar{\boldsymbol{u}}}_i(G_i)$ denotes the skew-symmetric matrix employed for defining the cross product with its axial vector $\bar{\boldsymbol{u}}_i(G_i)$, m_i indicates the mass of the body i, and $\bar{\boldsymbol{I}}_{G_i}$ is the symmetric inertia matrix of the generic rigid body i. The local position vector of the generic body center of mass $\bar{\boldsymbol{u}}_i(G_i)$ and the generic body inertia matrix $\bar{\boldsymbol{I}}_{G_i}$ are respectively defined as:

$$\bar{\boldsymbol{u}}_i(G_i) = \begin{bmatrix} \bar{x}_{G_i} \\ \bar{y}_{G_i} \\ \bar{z}_{G_i} \end{bmatrix}, \quad \bar{\boldsymbol{I}}_{G_i} = \begin{bmatrix} I_{xx,i} & I_{xy,i} & I_{xz,i} \\ I_{xy,i} & I_{yy,i} & I_{yz,i} \\ I_{xz,i} & I_{yz,i} & I_{zz,i} \end{bmatrix} \tag{21}$$

where $\bar{x}_{G_i}$, $\bar{y}_{G_i}$, and $\bar{z}_{G_i}$ denote the local coordinates of the center of mass of the generic rigid body i, while $I_{xx,i}$, $I_{yy,i}$, $I_{zz,i}$, $I_{xy,i}$, $I_{xz,i}$, and $I_{yz,i}$ represent the mass moments of inertia relative to the generic rigid body i. Considering the analytical form of the kinetic energy associated with the generic rigid body i and by using the principles of classical mechanics, the body mass matrix and the body inertia quadratic velocity vector, respectively denoted with $\boldsymbol{M}_i$ and $\boldsymbol{Q}_{v,i}$, can be obtained in an explicit form. By doing so, one can write the following matrix and vector quantities:

$$\boldsymbol{M}_i = \frac{\partial}{\partial \ddot{\boldsymbol{q}}_i} \left(\frac{d}{dt} \left(\frac{\partial T_i}{\partial \dot{\boldsymbol{q}}_i} \right)^T \right) = \begin{bmatrix} m_i \boldsymbol{I} & m_i \boldsymbol{A}_i \tilde{\bar{\boldsymbol{u}}}_i^T(G_i) \bar{\boldsymbol{G}}_i \\ m_i \bar{\boldsymbol{G}}_i^T \tilde{\bar{\boldsymbol{u}}}_i(G_i) \boldsymbol{A}_i^T & \bar{\boldsymbol{G}}_i^T \bar{\boldsymbol{I}}_{G_i} \bar{\boldsymbol{G}}_i \end{bmatrix} \tag{22}$$

and

$$\boldsymbol{Q}_{v,i} = \left(\frac{\partial T_i}{\partial \boldsymbol{q}_i} \right)^T - \dot{\boldsymbol{M}}_i \dot{\boldsymbol{q}}_i = \begin{bmatrix} m_i \boldsymbol{A}_i \tilde{\bar{\boldsymbol{\omega}}}_i \tilde{\bar{\boldsymbol{u}}}_i(G_i) \bar{\boldsymbol{\omega}}_i + m_i \boldsymbol{A}_i \tilde{\bar{\boldsymbol{u}}}_i(G_i) \dot{\bar{\boldsymbol{G}}}_i \dot{\boldsymbol{\theta}}_i \\ -\bar{\boldsymbol{G}}_i^T \tilde{\bar{\boldsymbol{\omega}}}_i \bar{\boldsymbol{I}}_{G_i} \bar{\boldsymbol{\omega}}_i - \bar{\boldsymbol{G}}_i^T \bar{\boldsymbol{I}}_{G_i} \dot{\bar{\boldsymbol{G}}}_i \dot{\boldsymbol{\theta}}_i \end{bmatrix} \tag{23}$$

where $\boldsymbol{I}$ is the 3×3 identity matrix. On the other hand, the four rigid bodies that form the bicycle multibody system are subjected to the gravity force field, representing the unique source of external forces for this mechanical system. Therefore, for a generic rigid body i, the generalized external force vector associated with the gravitational field is denoted with $\boldsymbol{Q}_{e,i}$ and can be analytically computed by using a Lagrangian approach leading to the following mathematical expression:

$$\boldsymbol{Q}_{e,i} = -\left(\frac{\partial U_i}{\partial \boldsymbol{q}_i} \right)^T = \begin{bmatrix} m_i \boldsymbol{g}_i \\ m_i \bar{\boldsymbol{G}}_i^T \tilde{\bar{\boldsymbol{u}}}_i(G_i) \boldsymbol{A}_i^T \boldsymbol{g}_i \end{bmatrix} \tag{24}$$

where $\boldsymbol{g}_i$ represents the gravity acceleration vector associated with the rigid body i that is defined as:

$$\boldsymbol{g}_i = \begin{bmatrix} 0 & 0 & -g \end{bmatrix}^T \tag{25}$$

At this stage, one can write straightforwardly the total body generalized force vector associated with the rigid body i that is denoted with $\boldsymbol{Q}_{b,i}$ as follows:

$$\boldsymbol{Q}_{b,i} = \boldsymbol{Q}_{v,i} + \boldsymbol{Q}_{e,i} \tag{26}$$

Furthermore, the total kinetic energy and the total potential energy of the bicycle system denoted with T and U, respectively, are obtained by summing the kinetic energy denoted with T_i and the potential energy denoted with U_i associated with the four rigid bodies that form the multibody system. Thus, one can write:

$$T = \sum_{i=1}^{4} T_i = T_1 + T_2 + T_3 + T_4, \quad U = \sum_{i=1}^{4} U_i = U_1 + U_2 + U_3 + U_4 \tag{27}$$

Consequently, the system total mass matrix indicated with $\boldsymbol{M}$ and the system total body generalized force vector denoted with $\boldsymbol{Q}_b$ relative to the bicycle multibody model can be derived in a block matrix form using a standard multibody assembly procedure leading to:

$$\boldsymbol{M} = \bigcup_{i=1}^{4} \boldsymbol{M}_i = \begin{bmatrix} \boldsymbol{M}_1 & \boldsymbol{O} & \boldsymbol{O} & \boldsymbol{O} \\ \boldsymbol{O} & \boldsymbol{M}_2 & \boldsymbol{O} & \boldsymbol{O} \\ \boldsymbol{O} & \boldsymbol{O} & \boldsymbol{M}_3 & \boldsymbol{O} \\ \boldsymbol{O} & \boldsymbol{O} & \boldsymbol{O} & \boldsymbol{M}_4 \end{bmatrix}, \quad \boldsymbol{Q}_b = \bigcup_{i=1}^{4} \boldsymbol{Q}_{b,i} = \begin{bmatrix} \boldsymbol{Q}_{b,1} \\ \boldsymbol{Q}_{b,2} \\ \boldsymbol{Q}_{b,3} \\ \boldsymbol{Q}_{b,4} \end{bmatrix} \tag{28}$$

For each rigid body i that forms the multibody model of the bicycle system, one can readily identify a set of ten independent inertial parameters associated with each body, which can be grouped in a parameter vector denoted with $\boldsymbol{b}_{i,i}$ and given by:

$$\boldsymbol{b}_{i,i} = \begin{bmatrix} \bar{x}_{G_i} & \bar{y}_{G_i} & \bar{z}_{G_i} & m_i & I_{xx,i} & I_{yy,i} & I_{zz,i} & I_{xy,i} & I_{xz,i} & I_{yz,i} \end{bmatrix}^T \tag{29}$$

Considering the entire dynamical model of the bicycle system, a comprehensive vector of inertial parameters denoted with $\boldsymbol{b}_i$ can be defined as follows:

$$\boldsymbol{b}_i = \begin{bmatrix} \boldsymbol{b}_{i,1} \\ \boldsymbol{b}_{i,2} \\ \boldsymbol{b}_{i,3} \\ \boldsymbol{b}_{i,4} \end{bmatrix} \tag{30}$$

where the multibody model of the Whipple-Carvallo bicycle system is obtained as an assembly of four rigid bodies and the vector of inertial parameters $\boldsymbol{b}_i$ is formed by $n_{b,i} = 40$ parameters. Therefore, the set of independent inertial parameters of the bicycle system is formed by forty parameters necessary to describe the dynamic effects captured by the multibody model. The system total mass matrix and the system total body generalized force vector serve to define the differential part in the equations of motion of the bicycle multibody model. The algebraic part of the equations of motion, on the other hand, arises from the definition of the constraint equations representing the kinematic joints and the contact conditions of the bicycle system.

2.4 Algebraic Constraints

In this subsection, the algebraic equations that serve to identify the kinematic constraints and the contact conditions of the bicycle system are provided. In the multibody model of the bicycle system, a set of n_c algebraic constraints is considered. The total set of n_c algebraic constraints encompasses $n_{c,h}$ holonomic constraints, that are used to model the mechanical joints which connect the rigid bodies of the bicycle multibody system as well as to define the motion imposed on the bicycle, and $n_{c,nh}$ nonholonomic constraints, which, on the other hand, serve to define the condition of pure rolling of the bicycle wheels. Considering the kinematic description of the motion of the rigid bodies that form the bicycle system and employing the bicycle parametric model discussed above, it is possible to define the holonomic and nonholonomic constraints of the multibody model devised for the bicycle system.

In the multibody model of the Whipple-Carvallo bicycle system developed in this paper, there are $n_{c,h} = 18$ holonomic constraint equations. The set of holonomic constraints models the motion imposed on the rear wheel, the kinematic joints that connect the mechanical parts that form the bicycle, and the contact constraints between the wheels and the ground. In addition, $n_{c,nh} = 4$ nonholonomic constraint equations that define the pure rolling conditions for both the rear and front wheels are also taken into account. In particular, the set of holonomic algebraic equations encompasses two contact constraints, three revolute joints, and a condition of imposed motion, while the set of nonholonomic algebraic equations is formed by two couples of conditions of rolling without slipping. In Table 2, all the geometric information needed to define the holonomic constraints of the bicycle multibody model is reported.

Table 2. Holonomic constraints of the bicycle multibody model.

Constraint number	Constraint type	First body	Second body	Collocation point	First body joint axis	Second body joint axis
1	Contact condition	Rear wheel	Ground	A	-	-
2	Imposed motion	Rear wheel	-	-	-	-
3	Revolute joint	Rear wheel	Rear frame	B	0,0,1	0,0,1
4	Revolute joint	Rear frame	Front frame	C	0,1,0	1,0,0
5	Revolute joint	Front frame	Front wheel	E	0,0,1	0,0,1
6	Contact condition	Front wheel	Ground	F	-	-

The first holonomic constraint equation is the contact between the rear wheel and the ground. The corresponding algebraic equation is:

$$C_1 = z_1 - R_r \sin(\psi_1) = 0 \tag{31}$$

where C_1 is the first holonomic constraint function and R_r is the radius of the rear wheel.

The second holonomic constraint equation represents the angular motion imposed at the rear wheel. The expression of the corresponding algebraic equation is:

$$C_2 = \psi_1 - \omega t = 0 \tag{32}$$

where C_2 is the second holonomic constraint function, t is time, and ω is the constant angular velocity imposed at the rear wheel.

As mentioned before, in the multibody model of the bicycle system, there are three revolute joints that are respectively collocated in the points B, C, and E shown in Figure 1. In particular, the first revolute joint collocated at the point B is interposed between the rear wheel and the rear frame. The second revolute joint collocated at the point C is interposed between the rear frame and the front frame. The third revolute joint collocated at the point E is interposed between the front frame and the front wheel. The complete expression of the holonomic algebraic equations representing a revolute joint can be written in a general and compact form as follows:

$$\boldsymbol{C}_k = \begin{bmatrix} \boldsymbol{r}_i(P) - \boldsymbol{r}_j(P) \\ \boldsymbol{v}_{2,i}^T \boldsymbol{v}_{1,j} \\ \boldsymbol{v}_{3,i}^T \boldsymbol{v}_{1,j} \end{bmatrix} = \boldsymbol{0}, \quad k = 3, 4, 5 \tag{33}$$

where $\boldsymbol{C}_k$ is the holonomic constraint vector associated with the revolute joint identified by the integer number k, the integer numbers respectively labeled with i, j, and k respectively represent the first and second body numbers involved in the kinematic pair, as well as the constraint number, while the point P represents the collocation point of the revolute joint, whereas the direction vectors $\boldsymbol{v}_{1,i}$ and $\boldsymbol{v}_{1,j}$ indicates the direction of the joint axis respectively represented with respect to the first and second bodies connected by the revolute joint, and the direction vectors $\boldsymbol{v}_{2,i}$, $\boldsymbol{v}_{3,i}$, $\boldsymbol{v}_{2,j}$, and $\boldsymbol{v}_{3,j}$ denote the two couples of vectors that are orthogonal to the joint axis respectively represented with respect to the first and second bodies of the kinematic joint.

The first revolute joint is interposed between the rear wheel and the rear frame and is collocated at the point B of Figure 1. Thus, the local position vectors of the point B, that are respectively defined with respect to the rear wheel local reference system and with respect to the rear frame local reference system, are respectively denoted with $\bar{\boldsymbol{u}}_1(B)$ and $\bar{\boldsymbol{u}}_2(B)$ and are given by:

$$\bar{\boldsymbol{u}}_1(B) = \begin{bmatrix} 0 \\ 0 \\ 0 \end{bmatrix}, \quad \bar{\boldsymbol{u}}_2(B) = \begin{bmatrix} -a_r \\ -c_r \\ 0 \end{bmatrix} \tag{34}$$

The second revolute joint is interposed between the rear frame and the front frame and is collocated at the point C of Figure 1. Thus, the local position vectors of the point C, that are respectively defined with respect to the rear frame local reference system and with respect to the front frame local reference system, are respectively denoted with $\bar{\boldsymbol{u}}_2(C)$ and $\bar{\boldsymbol{u}}_3(C)$ and are given by:

$$\bar{\boldsymbol{u}}_2(C) = \begin{bmatrix} b_r \\ -c_r \\ 0 \end{bmatrix}, \quad \bar{\boldsymbol{u}}_3(C) = \begin{bmatrix} -a_f \\ -c_f \\ 0 \end{bmatrix} \tag{35}$$

The third revolute joint is interposed between the front frame and the front wheel and is collocated at the point E of Figure 1. Thus, the local position vectors of the point E, that are respectively defined with respect to the front frame local reference system and with respect to the front wheel local reference system, are respectively denoted with $\bar{\boldsymbol{u}}_3(E)$ and $\bar{\boldsymbol{u}}_4(E)$ and are given by:

$$\bar{\boldsymbol{u}}_3(E) = \begin{bmatrix} b_f \\ -c_f \\ 0 \end{bmatrix}, \quad \bar{\boldsymbol{u}}_4(E) = \begin{bmatrix} 0 \\ 0 \\ 0 \end{bmatrix} \tag{36}$$

The sixth and last holonomic constraint is the algebraic equation modeling the contact between the front wheel and the ground. The corresponding constraint algebraic equation has the following expression:

$$C_6 = z_4 - R_f \sin(\psi_4) = 0 \tag{37}$$

where C_6 is the sixth holonomic constraint function. Thus, the total vector associated with the holonomic constraint equations denoted with $\boldsymbol{C}$ can be easily assembled as follows:

$$\boldsymbol{C} = \begin{bmatrix} C_1 & C_2 & \boldsymbol{C}_3^T & \boldsymbol{C}_4^T & \boldsymbol{C}_5^T & C_6 \end{bmatrix}^T \tag{38}$$

The total vector of holonomic constraint equations denoted with $\boldsymbol{C}$ is associated with a vector of holonomic Lagrange multipliers indicated with $\boldsymbol{\lambda}$ having dimensions $n_{c,h} = 18$. Starting from the total vector of holonomic constraint equations $\boldsymbol{C}$, one can compute through symbolic manipulations the total Jacobian matrix of the holonomic constraint equations denoted with $\boldsymbol{C_q}$ and the holonomic constraint quadratic velocity vector denoted with $\boldsymbol{Q}_{d,h}$.

The multibody model of the Whipple-Carvallo bicycle system involves the presence of two sets of nonholonomic algebraic constraint equations. The first set of nonholonomic constraints models the rolling without slipping of the rear wheel. The algebraic equations associated with the pure rolling constraints of the rear wheel are:

$$\boldsymbol{D}_1 = \begin{bmatrix} v_x(A) \\ v_y(A) \end{bmatrix} = \boldsymbol{0} \tag{39}$$

where $\boldsymbol{D}_1$ is the first nonholonomic constraint vector, while $v_x(A)$ and $v_y(A)$ respectively represent the longitudinal and the lateral velocities of the contact point A collocated on the rear wheel that are respectively given by:

$$\begin{cases} v_x(A) = \dot{x}_1 + R_r \dot{\psi}_1 \cos(\vartheta_1) \\ \\ v_y(A) = \dot{y}_1 + R_r \dot{\phi}_1 \sin(\phi_1) + R_r \dot{\psi}_1 \sin(\phi_1) \sin(\vartheta_1) \end{cases} \tag{40}$$

The second set of nonholonomic constraints models the rolling without slipping of the front wheel. By using the same approach, the algebraic equations relative to the pure rolling constraints of the front wheel can be defined as:

$$\boldsymbol{D}_2 = \begin{bmatrix} v_x(F) \\ v_y(F) \end{bmatrix} = \boldsymbol{0} \tag{41}$$

where $\boldsymbol{D}_2$ is the second nonholonomic constraint vector, while $v_x(F)$ and $v_y(F)$ respectively represent the longitudinal and the lateral velocities of the contact point F collocated on the front wheel that are respectively given by:

$$\begin{cases} v_x(F) = \dot{x}_4 + R_f \dot{\psi}_4 \cos(\vartheta_4) \\ \\ v_y(F) = \dot{y}_4 + R_f \dot{\phi}_4 \sin(\phi_4) + R_f \dot{\psi}_4 \sin(\phi_4) \sin(\vartheta_4) \end{cases} \tag{42}$$

Consequently, the total vector associated with the nonholonomic constraint equations denoted with $\boldsymbol{D}$ can be readily assembled as follows:

$$\boldsymbol{D} = \begin{bmatrix} \boldsymbol{D}_1 \\ \boldsymbol{D}_2 \end{bmatrix} \tag{43}$$

The total vector of nonholonomic constraint equations denoted with $\boldsymbol{D}$ is associated with a vector of nonholonomic Lagrange multipliers indicated with $\boldsymbol{\mu}$ having dimensions $n_{c,nh} = 4$. By manipulating the total vector of nonholonomic constraint equations $\boldsymbol{D}$, one can calculate the total Jacobian matrix of the nonholonomic constraint equations indicated with $\boldsymbol{D_{\dot{q}}}$ and the nonholonomic constraint quadratic velocity vector indicated with $\boldsymbol{Q}_{d,nh}$.

At this stage, the complete vector of holonomic and nonholonomic algebraic constraints can be identified. For this purpose, the total vector of algebraic constraints indicated with $\boldsymbol{E}$ can be formally written as:

$$\boldsymbol{E} = \begin{bmatrix} \boldsymbol{C}^T & \boldsymbol{D}^T \end{bmatrix}^T = \begin{bmatrix} C_1 & C_2 & \boldsymbol{C}_3^T & \boldsymbol{C}_4^T & \boldsymbol{C}_5^T & C_6 & \boldsymbol{D}_1^T & \boldsymbol{D}_2^T \end{bmatrix}^T \tag{44}$$

The total vector of algebraic constraint equations denoted with $\boldsymbol{E}$ is associated with a vector of holonomic and nonholonomic Lagrange multipliers indicated with $\boldsymbol{v}$ having dimensions $n_c = 22$. To complete the algebraic part of the multibody model, the total Jacobian matrix of the algebraic constraint equations denoted with $\boldsymbol{J}$ and the total quadratic velocity vector associated with the algebraic constraints indicated with $\boldsymbol{Q}_d$ are required. These matrix and vector quantities can be directly obtained by assembling the analytical expressions provided above.

The derivation of the algebraic equations associated with the holonomic and nonholonomic constraints completes the description of the bicycle multibody model. Thus, starting from the nonlinear form of the differential-algebraic equations of motion of the multibody system at hand, and by using the linearization procedure described in detail in the manuscript, one can readily obtain a linearized model of the Whipple-Carvallo bicycle system characterized by the composite mass, damping, and stiffness matrices respectively denoted with $\bar{\boldsymbol{M}}$, $\bar{\boldsymbol{R}}$, and $\bar{\boldsymbol{K}}$. After that, the composite mass, damping, and stiffness matrices can be particularized in the generalized configuration of interest for the stability problem, leading to the special formulation of the generalized eigenvalue problem applied in this paper to bicycle systems [64]. By doing so, both the nonlinear and the linearized dynamic models are expressed in a parametric form suitable for performing dynamic analysis and stability studies in several scenarios of practical engineering interest, as shown in detail in the numerical results section of the paper.

3. Numerical Results and Discussion

In this section, the numerical results concerning linear and nonlinear stability studies carried out on the bicycle multibody model obtained using the analytical and numerical approaches devised in the paper are presented.

3.1 Bicycle Model Parameters

In this subsection, the process for obtaining the numerical parameters employed for the computer implementation of the bicycle multibody model of interest for this paper is described. The first important step for performing numerical experiments using the multibody model of the Whipple-Carvallo bicycle system developed in this work consists of defining the set of model parameters necessary for describing the mechanical system of interest and to identify consistent numerical values for these parameters. This fundamental step is necessary to perform numerical experiments based on the mathematical model of the bicycle system leading to physically meaningful numerical results. As discussed in the paper, the present bicycle multibody model is based on a set of geometric parameters denoted with $\boldsymbol{b}_g$, as well as on a set of inertial parameters denoted with $\boldsymbol{b}_i$. Therefore, the total set of model parameters for the bicycle is indicated with $\boldsymbol{b}$ and is defined as:

$$\boldsymbol{b} = \begin{bmatrix} \boldsymbol{b}_g \\ \boldsymbol{b}_i \end{bmatrix} \tag{45}$$

where the parameter vector $\boldsymbol{b}$ is formed by $n_b = n_{b,g} + n_{b,i} = 6 + 40 = 46$ model parameters.

The numerical values for the vector of model parameter denoted with $\boldsymbol{b}$ identified before can be obtained by comparing the bicycle multibody model developed in this work with the simplified dynamical model found in the literature that is assumed as the benchmark. Considering these two dynamical models, an important difference to be outlined between the benchmark bicycle model and the proposed bicycle model is the diverse orientation of the inertial reference system and the local reference systems of each body. In particular, the inertial reference system employed in the proposed multibody model has a different orientation when compared with respect to the inertial reference system of the benchmark model.

To solve the data conversion problem, a two-step process must be performed. First, a rotation of the global reference system used in the benchmark model must be carried out about the X axis of an angle equal to $\alpha_{b,1} = \pi$ to obtain the orientation of the global frame of reference of the present multibody model. Second, the local reference systems of the bicycle multibody model developed in this work also have different orientations when compared with respect to the local reference systems of the benchmark model. Thus, similarly to the previous process, this problem must be solved by considering as a second step an additional rotation of the local reference systems about the X axis of an angle denoted with $\alpha_{b,2} = \pi/2$. This two-step transformation process is important to properly convert the inertia tensors of the benchmark bicycle model in accordance with the local reference systems employed in the case of the present multibody model. It is, therefore, apparent that a total rotation of $\alpha_b = \alpha_{b,1} + \alpha_{b,2} = 3\pi/2$ performed about the global axis X is required for the data conversion. For this purpose, the following linear transformation can be used to obtain a consistent inertia matrix for each body i starting from the inertia matrix of the benchmark bicycle model:

$$\bar{\boldsymbol{I}}_{G_i} = \boldsymbol{A}_{X,b}^T \bar{\boldsymbol{I}}_{G_i,b} \boldsymbol{A}_{X,b} \tag{46}$$

where $\bar{\boldsymbol{I}}_{G_i}$ is the inertia matrix of the generic body i of the proposed bicycle multibody model expressed in its local reference system, $\bar{\boldsymbol{I}}_{G_i,b}$ is the inertia matrix of the generic body i of the benchmark bicycle model defined in its local reference system, and $\boldsymbol{A}_{X,b}$ is the rotation matrix that depends on the angle α_b and serves to transform the data between the two dynamical models correctly. The conversion matrix $\boldsymbol{A}_{X,b}$ can be explicitly written as:

$$\boldsymbol{A}_{X,b} = \begin{bmatrix} 1 & 0 & 0 \\ 0 & \cos(\alpha_b) & -\sin(\alpha_b) \\ 0 & \sin(\alpha_b) & \cos(\alpha_b) \end{bmatrix} = \begin{bmatrix} 1 & 0 & 0 \\ 0 & 0 & 1 \\ 0 & -1 & 0 \end{bmatrix} \tag{47}$$

where $\alpha_b = 3\pi/2$, as mentioned before. By implementing the conversion process of the inertia matrix associated with each rigid body of the bicycle system described before and by analyzing the bicycle benchmark model employed as a reference found in the literature, the numerical values for the model parameter vector $\boldsymbol{b}$ of the present multibody model can be obtained. The values of the numerical parameters encapsulated in the parameter vector $\boldsymbol{b}$, together with additional numerical parameters of interest for the bicycle multibody model considered in this work, are reported in Table 3.

The numerical data used for the proposed bicycle multibody model that are reported in Table 3 arise from the adaptation to the problem at of the numerical data of the bicycle benchmark model that can be found in reference [4]. To perform a systematic analysis of the multibody model of the bicycle system developed in this paper, the case of the Whipple-Carvallo bicycle system without the presence of the rider is considered as well. For simplicity, this second case of interest is referred to as the riderless bicycle system. The numerical values of the physical parameters that completely describe the multibody model of the riderless bicycle system are extracted from the reference benchmark models found in the literature by using the same conversion procedure described above in the bicycle with the rider. By doing so, the parameters of interest for the riderless bicycle model are derived, as reported in Table 4.

Table 3. Bicycle model parameters.

Description	Symbol	Data (units)
Rear wheel radius	R_r	0.3 (m)
Front wheel radius	R_f	0.35 (m)
Wheelbase	W_b	1.02 (m)
Fork offset	H_f	0.0321 (m)
Rear frame angle	β	0.3142 (rad)
Caster angle	ε	0.3142 (rad)
Geometric trail	T_b	0.08 (m)
Rear frame length	L_r	0.953 (m)
Rear frame first distance	a_r	0.471 (m)
Rear frame second distance	b_r	0.483 (m)
Rear frame third distance	c_r	0.478 (m)
Front frame length	L_f	0.268 (m)
Front frame first distance	a_f	-0.102 (m)
Front frame second distance	b_f	0.370 (m)
Front frame third distance	c_f	0.026 (m)
Rear wheel centroid vector	$\boldsymbol{R}_1 = \begin{bmatrix} x_1 & 0 & z_1 \end{bmatrix}^T$	$\begin{bmatrix} 0 & 0 & 0.3 \end{bmatrix}^T$ (m)
Rear frame centroid vector	$\boldsymbol{R}_2 = \begin{bmatrix} x_2 & 0 & z_2 \end{bmatrix}^T$	$\begin{bmatrix} 0.3 & 0 & 0.9 \end{bmatrix}^T$ (m)
Front frame centroid vector	$\boldsymbol{R}_3 = \begin{bmatrix} x_3 & 0 & z_3 \end{bmatrix}^T$	$\begin{bmatrix} 0.9 & 0 & 0.7 \end{bmatrix}^T$ (m)
Front wheel centroid vector	$\boldsymbol{R}_4 = \begin{bmatrix} x_4 & 0 & z_4 \end{bmatrix}^T$	$\begin{bmatrix} 1.02 & 0 & 0.35 \end{bmatrix}^T$ (m)
Rear wheel mass	m_1	2 (kg)
Rear frame mass	m_2	85 (kg)
Front frame mass	m_3	4 (kg)
Front wheel mass	m_4	3 (kg)
Rear wheel inertia matrix	$\bar{\boldsymbol{I}}_{G_1} = \begin{bmatrix} I_{xx,1} & 0 & 0 \\ 0 & I_{yy,1} & 0 \\ 0 & 0 & I_{zz,1} \end{bmatrix}$	$\begin{bmatrix} 6.03 \cdot 10^{-2} & 0 & 0 \\ 0 & 6.03 \cdot 10^{-2} & 0 \\ 0 & 0 & 1.2 \cdot 10^{-1} \end{bmatrix}$ (kg × m^2)
Rear frame inertia matrix	$\bar{\boldsymbol{I}}_{G_2} = \begin{bmatrix} I_{xx,2} & I_{xy,2} & 0 \\ I_{xy,2} & I_{yy,2} & 0 \\ 0 & 0 & I_{zz,2} \end{bmatrix}$	$\begin{bmatrix} 7.178 & -3.822 & 0 \\ -3.822 & 4.822 & 0 \\ 0 & 0 & 11 \end{bmatrix}$ (kg × m^2)
Front frame inertia matrix	$\bar{\boldsymbol{I}}_{G_3} = \begin{bmatrix} I_{xx,3} & I_{xy,3} & 0 \\ I_{xy,3} & I_{yy,3} & 0 \\ 0 & 0 & I_{zz,3} \end{bmatrix}$	$\begin{bmatrix} 7.587 \cdot 10^{-3} & 9.119 \cdot 10^{-3} & 0 \\ 9.119 \cdot 10^{-3} & 5.841 \cdot 10^{-2} & 0 \\ 0 & 0 & 6 \cdot 10^{-2} \end{bmatrix}$ (kg × m^2)
Front wheel inertia matrix	$\bar{\boldsymbol{I}}_{G_4} = \begin{bmatrix} I_{xx,4} & 0 & 0 \\ 0 & I_{yy,4} & 0 \\ 0 & 0 & I_{zz,4} \end{bmatrix}$	$\begin{bmatrix} 1.405 \cdot 10^{-1} & 0 & 0 \\ 0 & 1.405 \cdot 10^{-1} & 0 \\ 0 & 0 & 2.8 \cdot 10^{-1} \end{bmatrix}$ (kg × m^2)

The numerical data employed for the proposed riderless bicycle multibody model that are summarized in Table 4 derive from the adjustment to the problem under consideration of the numerical data of the riderless bicycle benchmark model provided in reference [5]. As can be noted by observing the data reported in Tables 3 and 4, the numerical values of the physical parameters used in the case of the riderless bicycle model are substantially diverse from those employed in the case of the bicycle with the rider. The largest difference between the two bicycle models is in the reduced mass of the rear frame. However, adopting the general stability analysis method discussed in this paper, the bicycle benchmark multibody model with the rider and the bicycle benchmark multibody model without the rider can be equally employed for studying the stability characteristics of this mechanical system through numerical experiments.

3.2 Linear Stability Analysis

In this subsection, the linear stability analysis of the motion along a straight line of the bicycle multibody model is performed. The numerical results found are compared with those available in the literature. The multibody model developed in this work is used to reproduce the numerical results of the benchmark bicycle models found in the literature to verify the physical consistency of the dynamical behavior captured by the proposed multibody model [4,5]. To this end, the multibody model proposed in this work for the Whipple-Carvallo bicycle system is implemented in MATLAB by developing a general-purpose multibody computer program based on a procedural approach that is consistent with the logic of this powerful multiparadigm numerical computing environment. A mixed symbolic/numerical approach is adopted to facilitate the mathematical derivation of the nonlinear differential-algebraic equations of motion and the subsequent linearization process. The equations of motion can be readily obtained and can be systematically linearized in a symbolic form following the analytical methodology devised in this paper. Once the motion equations are obtained in both their nonlinear and linearized forms, they are systematically transformed into a set of computer subroutines suitable for performing numerical experiments.

By using the numerical data for the model parameters reported in Table 3, the numerical results obtained employing the proposed multibody model in the case of the linear stability analysis can be compared with those arising from the benchmark model

Table 4. Riderless bicycle model parameters.

Description	Symbol	Data (units)
Rear wheel radius	R_r	0.3500 (m)
Front wheel radius	R_f	0.3485 (m)
Wheelbase	W_b	1.01 (m)
Fork offset	H_f	-0.5249 (m)
Rear frame angle	β	0.3665 (rad)
Caster angle	ε	0.3665 (rad)
Geometric trail	T_b	0.190 (m)
Rear frame length	L_r	0.9949 (m)
Rear frame first distance	a_r	0.3980 (m)
Rear frame second distance	b_r	0.5968 (m)
Rear frame third distance	c_r	0.1439 (m)
Front frame length	L_f	0.3633 (m)
Front frame first distance	a_f	-0.0951 (m)
Front frame second distance	b_f	0.4584 (m)
Front frame third distance	c_f	0.0131 (m)
Rear wheel centroid vector	$\boldsymbol{R}_1 = \begin{bmatrix} x_1 & 0 & z_1 \end{bmatrix}^T$	$\begin{bmatrix} 0 & 0 & 0.3500 \end{bmatrix}^T$ (m)
Rear frame centroid vector	$\boldsymbol{R}_2 = \begin{bmatrix} x_2 & 0 & z_2 \end{bmatrix}^T$	$\begin{bmatrix} 0.320 & 0 & 0.627 \end{bmatrix}^T$ (m)
Front frame centroid vector	$\boldsymbol{R}_3 = \begin{bmatrix} x_3 & 0 & z_3 \end{bmatrix}^T$	$\begin{bmatrix} 0.907 & 0 & 0.8 \end{bmatrix}^T$ (m)
Front wheel centroid vector	$\boldsymbol{R}_4 = \begin{bmatrix} x_4 & 0 & z_4 \end{bmatrix}^T$	$\begin{bmatrix} 1.01 & 0 & 0.3485 \end{bmatrix}^T$ (m)
Rear wheel mass	m_1	2.56 (kg)
Rear frame mass	m_2	12.06 (kg)
Front frame mass	m_3	2.54 (kg)
Front wheel mass	m_4	2.05 (kg)
Rear wheel inertia matrix	$\bar{\boldsymbol{I}}_{G_1} = \begin{bmatrix} I_{xx,1} & 0 & 0 \\ 0 & I_{yy,1} & 0 \\ 0 & 0 & I_{zz,1} \end{bmatrix}$	$\begin{bmatrix} 7.8 \cdot 10^{-2} & 0 & 0 \\ 0 & 7.8 \cdot 10^{-2} & 0 \\ 0 & 0 & 1.56 \cdot 10^{-1} \end{bmatrix}$ (kg $\times$ m^2)
Rear frame inertia matrix	$\bar{\boldsymbol{I}}_{G_2} = \begin{bmatrix} I_{xx,2} & I_{xy,2} & 0 \\ I_{xy,2} & I_{yy,2} & 0 \\ 0 & 0 & I_{zz,2} \end{bmatrix}$	$\begin{bmatrix} 8.279 \cdot 10^{-1} & 6.50 \cdot 10^{-2} & 0 \\ 6.50 \cdot 10^{-2} & 1.0700 & 0 \\ 0 & 0 & 1.2 \end{bmatrix}$ (kg $\times$ m^2)
Front frame inertia matrix	$\bar{\boldsymbol{I}}_{G_3} = \begin{bmatrix} I_{xx,3} & I_{xy,3} & 0 \\ I_{xy,3} & I_{yy,3} & 0 \\ 0 & 0 & I_{zz,3} \end{bmatrix}$	$\begin{bmatrix} 4.964 \cdot 10^{-3} & 6.658 \cdot 10^{-6} & 0 \\ 6.658 \cdot 10^{-6} & 9.793 \cdot 10^{-2} & 0 \\ 0 & 0 & 0.1 \end{bmatrix}$ (kg $\times$ m^2)
Front wheel inertia matrix	$\bar{\boldsymbol{I}}_{G_4} = \begin{bmatrix} I_{xx,4} & 0 & 0 \\ 0 & I_{yy,4} & 0 \\ 0 & 0 & I_{zz,4} \end{bmatrix}$	$\begin{bmatrix} 8.1 \cdot 10^{-2} & 0 & 0 \\ 0 & 8.1 \cdot 10^{-2} & 0 \\ 0 & 0 & 1.62 \cdot 10^{-1} \end{bmatrix}$ (kg $\times$ m^2)

of the Whipple-Carvallo bicycle system [4]. In Figure 3, the graphical comparison between the stability map obtained from the proposed multibody model and the stability map arising from the use of the benchmark bicycle model with the rider is represented.

In Figure 3, the variable v reported on the horizontal axis represents the linear forward velocity of the center of mass of the bicycle rear wheel that can be computed starting from the angular velocity ω imposed on the rear wheel as $v = R_r\omega$. On the vertical axis of Figure 3, on the other hand, the real and imaginary parts of the eigenvalues resulting from the two dynamical models of the Whipple-Carvallo bicycle system are respectively represented, that is, the linear version of the proposed bicycle multibody model and the benchmark bicycle model are respectively employed for computing the numerical results represented in Figure 3. In particular, three types of linear motions associated with three different families of eigenvalues can be distinguished in Figure 3. Namely, the castering eigenmode, the capsize eigenmode, and the weave eigenmode. To perform a systematic comparison, in Table 5, the errors between the eigenvalues obtained in the case of three different longitudinal velocities are reported for the two dynamical models considered.

By observing both Figure 3 and Table 5, the two eigenmodes that are usually referenced as the capsize mode and the weave mode are particularly interesting. While the weave mode corresponds to an oscillatory motion, the capsize mode is a nonoscillatory eigenmode. Considering the complex dynamical behavior of the bicycle system, these two modes are of paramount importance since they are responsible for the stability of this mechanical system. In fact, as shown in Figure 3, the so-called stability zone of the Whipple-Carvallo bicycle system is delimited by two important values of the forward velocity, which are the weave critical velocity equal to $v_{w,c} \approx 4.3$ (m/s) and the capsize critical velocity equal to $v_{c,c} \approx 6.0$ (m/s). In general, the amplitude of the stability region and the values of the two critical velocities depend on the geometric and inertial properties of the bicycle system, as discussed below.

Since the multibody model of the bicycle system developed in this work is based on a parametric structure, it can be effectively employed to analyze several dynamical scenarios of interest for engineering applications. For example, in the case of developing a nonlinear controller for improving the stability characteristics of an autonomous bicycle, one is interested in identifying the stability region of the riderless bicycle model. To demonstrate this fact through a simple numerical example, consider the case of the riderless

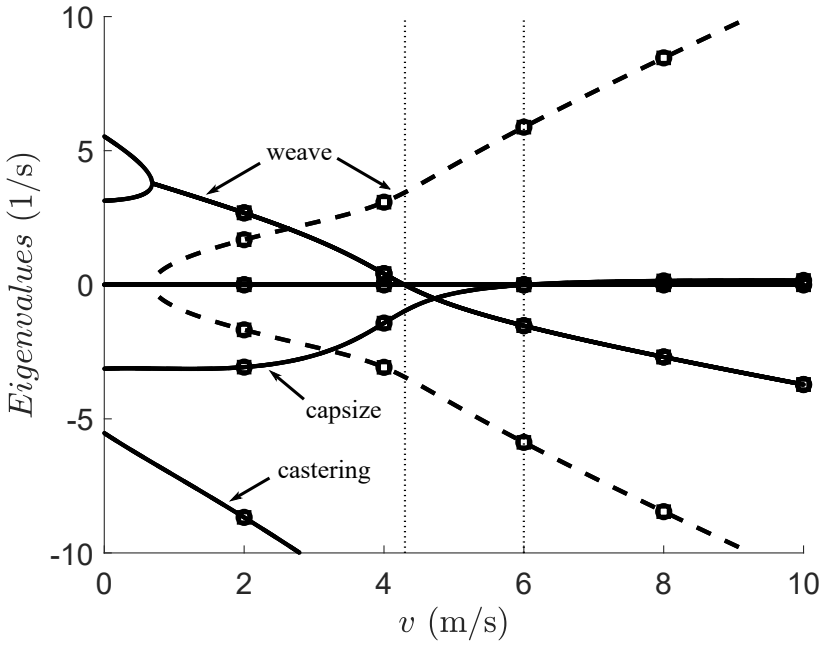

Figure 3. *Comparison of the stability maps of the bicycle models: eigenvalues and eigenmodes of the proposed bicycle multibody model compared with those of the linear benchmark bicycle model. The solid line (——) with circle markers (○) represents the real part of the eigenvalues calculated using the linear benchmark bicycle model. The solid line (——) with square markers (□) represents the real part of the eigenvalues calculated by linearizing the proposed bicycle multibody model. The dashed line (- - -) with circle markers (○) represents the imaginary part of the eigenvalues calculated using the linear benchmark bicycle model. The dashed line (- - -) with square markers (□) represents the imaginary part of the eigenvalues calculated by linearizing the proposed bicycle multibody model. The stable regions of the stability maps of the two bicycle models are denoted with two dotted vertical lines (·····).*

Table 5. Errors between the eigenvalues calculated by linearizing the proposed bicycle multibody model and the eigenvalues calculated using the linear benchmark bicycle model.

Eigenmodes	**Eigenvalues** $v = 1(m/s)$	**Eigenvalues** $v = 5(m/s)$	**Eigenvalues** $v = 10(m/s)$
Castering (real part)	$5,42 \cdot 10^{-14}$	$-4,6 \cdot 10^{-13}$	$-5,5 \cdot 10^{-13}$
Capsize (real part)	$9,33 \cdot 10^{-15}$	$9,13 \cdot 10^{-14}$	$3,16 \cdot 10^{-13}$
Weave (real part)	$5,77 \cdot 10^{-15}$	$6,31 \cdot 10^{-14}$	$-3,5 \cdot 10^{-13}$
Weave (imaginary part)	$2,22 \cdot 10^{-15}$	$2,84 \cdot 10^{-14}$	$-1,5 \cdot 10^{-12}$

bicycle multibody system that is obtained by reducing the mass of the rear frame and employing the numerical values of the system parameters reported in Table 4. By adopting a numerical procedure for the stability analysis identical to the one described above, the stability map of the riderless bicycle system can be obtained and the numerical results found can be readily compared with those produced by using the benchmark riderless bicycle model [5]. Thus, in the riderless bicycle system, the graphical comparison between the stability map determined by using the proposed multibody model and the stability map obtained from the use of the benchmark bicycle model is represented in Figure 4.

As shown in Figure 4, the riderless bicycle multibody model for the Whipple-Carvallo bicycle system exhibits the same eigenmodes associated with the linear dynamical behavior of the bicycle with the rider, which are again identified as the castering eigenmode, the capsize eigenmode, and the weave eigenmode. To quantitatively compare the proposed riderless bicycle model and the benchmark riderless bicycle model, Table 6 contains the errors between the eigenvalues found in the correspondence of the three different forward velocities of the two models of the riderless bicycle system. By analyzing the stability map of the riderless

Table 6. Errors between the eigenvalues calculated by linearizing the proposed riderless bicycle multibody model and the eigenvalues calculated using the linear benchmark riderless bicycle model.

Eigenmodes	**Eigenvalues** $v = 1(m/s)$	**Eigenvalues** $v = 5(m/s)$	**Eigenvalues** $v = 10(m/s)$
Castering (real part)	$5,06 \cdot 10^{-14}$	$2,86 \cdot 10^{-13}$	$1,63 \cdot 10^{-13}$
Capsize (real part)	$-1,69 \cdot 10^{-14}$	$-1,67 \cdot 10^{-15}$	$2,62 \cdot 10^{-13}$
Weave (real part)	$-4,44 \cdot 10^{-16}$	$-8,88 \cdot 10^{-16}$	$-8,86 \cdot 10^{-16}$
Weave (imaginary part)	$8,99 \cdot 10^{-15}$	$5,42 \cdot 10^{-14}$	$6,22 \cdot 10^{-13}$

bicycle model, the same dynamical behavior observed in the case of the regular bicycle model is found. However, the stability zone of the second benchmark model is different from the one of the first benchmark model since the two bicycle systems have diverse geometric shapes and feature different mass distributions. In fact, the stability zone of the Whipple-Carvallo bicycle system in absence of the rider is delimited between the weave critical velocity equal to $v_{w,c} \approx 3.99$ (m/s) and the capsize critical velocity equal to $v_{c,c} \approx 7.90$ (m/s), thereby leading to a wider stability region.

As demonstrated by analyzing Figures 3 and 4, as well as by observing the data reported in Tables 5 and 6, both devoted to the

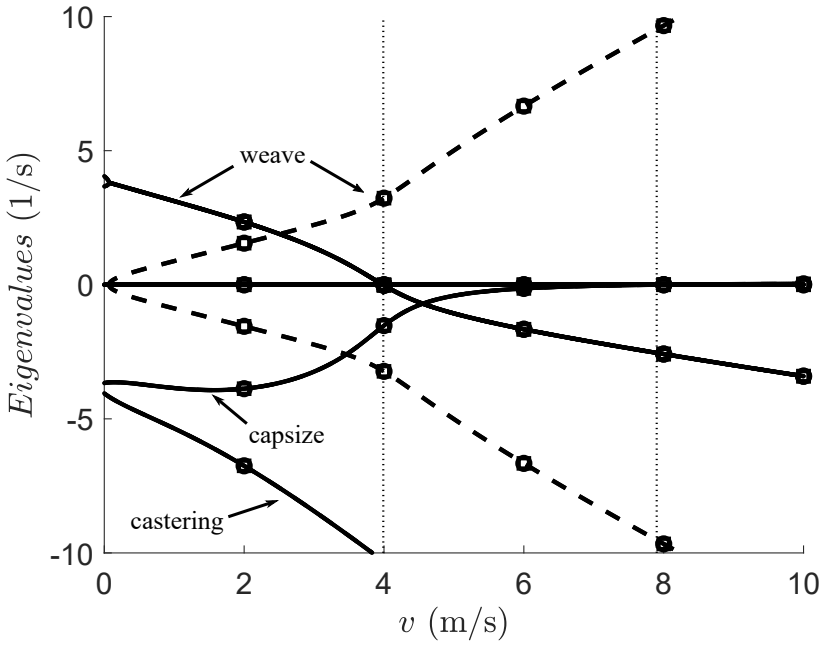

Figure 4. *Comparison of the stability maps of the riderless bicycle models: eigenvalues and eigenmodes of the proposed riderless bicycle multibody model compared with those of the linear benchmark riderless bicycle model. The solid line (——) with circle markers (○) represents the real part of the eigenvalues calculated using the linear benchmark riderless bicycle model. The solid line (——) with square markers (□) represents the real part of the eigenvalues calculated by linearizing the proposed riderless bicycle multibody model. The dashed line (- - -) with circle markers (○) represents the imaginary part of the eigenvalues calculated using the linear benchmark riderless bicycle model. The dashed line (- - -) with square markers (□) represents the imaginary part of the eigenvalues calculated by linearizing the proposed riderless bicycle multibody model. The stable regions of the stability maps of the two riderless bicycle models are denoted with two dotted vertical lines (·····).*

comparison between the linearized multibody models of the bicycle system developed in this work and the linear dynamical models typically assumed as the benchmark models for the Whipple-Carvallo bicycle system, the numerical results found are almost the same of the benchmark numerical results, since they only differ for round-off errors. Thus, the fact that the numerical results found in this paper are in a perfect agreement with those arising from the benchmark bicycle models demonstrates the generality and the effectiveness of the analysis method proposed in this investigation.

3.3 Nonlinear Stability Analysis

In this subsection, a nonlinear stability analysis is performed using the proposed bicycle multibody model. The numerical results found are compared with those obtained from the benchmark bicycle system with and without the rider. For this purpose, the dynamics of the proposed nonlinear bicycle model and the linear benchmark models are compared to show the different behavior of the two systems in response to a perturbation from the configuration of dynamic equilibrium. As expected, the differences in the dynamic behaviors of the two bicycle models are strictly related to the amplitudes of the perturbations given from the configuration of dynamic equilibrium. In general, one expects that, for small perturbations around the dynamic equilibrium configuration, the complex nonlinear model and the simplified linear model of the bicycle system should provide approximately the same set of numerical results, while the dynamic behaviors of the two models should qualitatively exhibit more apparent differences in the case of larger disturbances. Thus, the linear and nonlinear models of the Whipple-Carvallo bicycle system can be properly compared to highlight the differences in their dynamic behaviors mentioned before.

To demonstrate this fact through numerical experiments, an appropriate forward velocity denoted with v is assigned to the bicycle multibody model to obtain a stable dynamical behavior. Thus, the case in which the bicycle system can handle an external disturbance without falling is considered. The two dynamical models of the Whipple-Carvallo bicycle system are perturbed from the standard configuration of dynamic equilibrium employed for the stability analysis by imposing in the set of the initial conditions a disturbance of the initial roll rate denoted with $\dot{\phi}$. Subsequently, the time histories of the roll angle ϕ and of the steering angle δ resulting from the presence of the perturbation of the initial conditions are evaluated with the use of the two dynamical models, and their time evolutions are compared. Considering the bicycle system with the rider, the numerical results found for both the dynamical models in the case of two amplitudes of the perturbation are respectively represented in Figures 5 and 6.

In Figures 5a and 5b, the numerical results obtained for an initial roll rate equal to $\dot{\phi}_0 = 0.1$ (rad/s) and for an initial roll rate equal to $\dot{\phi}_0 = 0.5$ (rad/s) are respectively shown considering the time histories of the roll angle ϕ resulting from the comparison of the dynamical behavior of the proposed nonlinear bicycle model and the linear benchmark bicycle model. Similarly, Figures 6a and 6b show the time histories of the steering angle δ resulting from the comparison of the proposed nonlinear bicycle model and the linear benchmark bicycle model in the case of the same set of initial perturbations mentioned before. In this numerical experiment, the bicycle longitudinal velocity used for carrying out the numerical integration of the equations of motion employing the multibody computational procedure developed in this work is $v = 5$ (m/s). Consequently, being the radius of the rear wheel of the bicycle equal to $R_r = 0.30$ (m), the angular velocity employed in the case of the bicycle system with the rider is $\omega = 16.67$ (rad/s).

Considering the bicycle system without the rider, the numerical results obtained for both the dynamical models in the case of two amplitudes of the perturbation are represented in Figures 7 and 8, respectively.

In Figures 7a and 7b, the numerical results obtained for an initial roll rate equal to $\dot{\phi}_0 = 0.1$ (rad/s) and for an initial roll rate equal to $\dot{\phi}_0 = 1.0$ (rad/s) are respectively shown considering the time histories of the roll angle ϕ resulting from the comparison of the dynamical behavior of the proposed nonlinear riderless bicycle model and the linear benchmark riderless bicycle model. Similarly, Figures 8a and 8b show the time histories of the steering angle δ resulting from the comparison of the proposed nonlinear riderless bicycle model and the linear benchmark riderless bicycle model in the case of the same set of initial perturbations mentioned before.

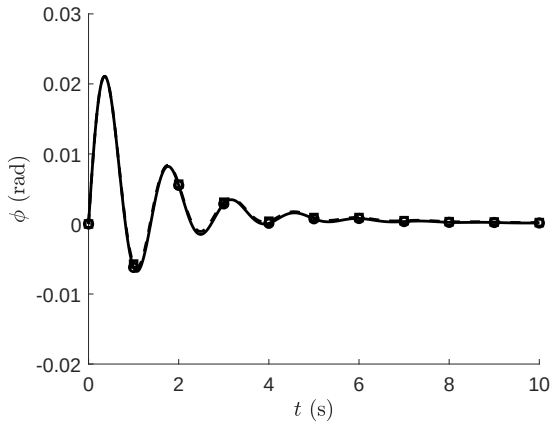

(a) *Roll angle obtained for an initial roll rate equal to* $\dot{\phi}_0 = 0.1$ *(rad/s) and using a longitudinal velocity equal to* $v = 5$ *(m/s).*

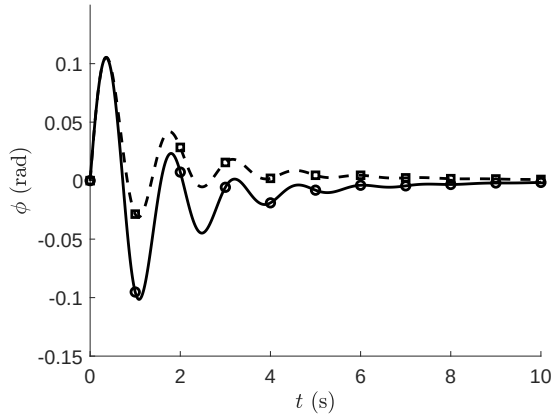

(b) *Roll angle obtained for an initial roll rate equal to* $\dot{\phi}_0 = 0.5$ *(rad/s) and using a longitudinal velocity equal to* $v = 5$ *(m/s).*

Figure 5. *Comparison of the dynamical behaviors of the linear and nonlinear bicycle models resulting from a perturbation of the configuration of dynamic equilibrium: roll angular displacement of the proposed nonlinear bicycle multibody model compared with the roll angle of the linear benchmark bicycle model. The solid line (——) with circle markers* (○) *represents the roll angle of the bicycle system calculated using the proposed nonlinear multibody model. The dashed line (- - -) with square markers* (□) *represents the roll angle of the bicycle system calculated employing the linear benchmark dynamic model.*

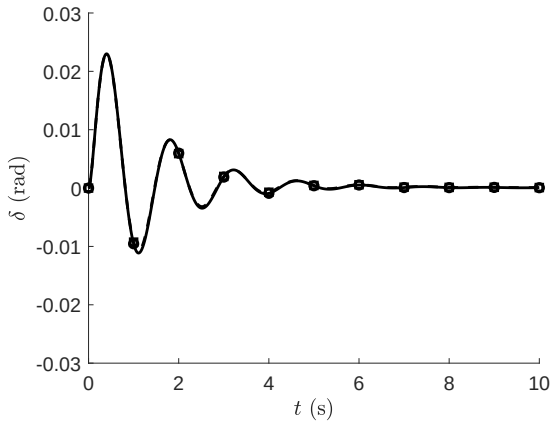

(a) *Steering angle obtained for an initial roll rate equal to* $\dot{\phi}_0 = 0.1$ *(rad/s) and using a longitudinal velocity equal to* $v = 5$ *(m/s).*

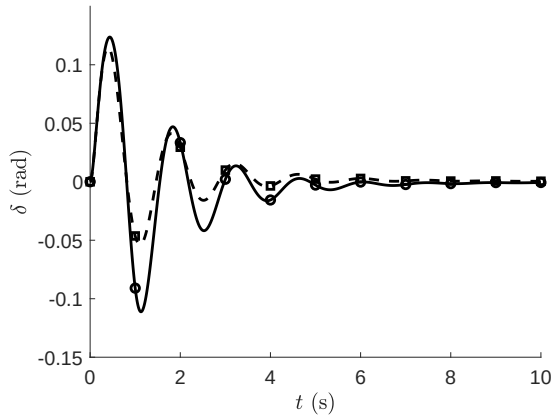

(b) *Steering angle obtained for an initial roll rate equal to* $\dot{\phi}_0 = 0.5$ *(rad/s) and using a longitudinal velocity equal to* $v = 5$ *(m/s).*

Figure 6. *Comparison of the dynamical behaviors of the linear and nonlinear bicycle models resulting from a perturbation of the configuration of dynamic equilibrium: steering angular displacement of the proposed nonlinear bicycle multibody model compared with the steering angle of the linear benchmark bicycle model. The solid line (——) with circle markers* (○) *represents the steering angle of the bicycle system calculated using the proposed nonlinear multibody model. The dashed line (- - -) with square markers* (□) *represents the steering angle of the bicycle system calculated employing the linear benchmark dynamic model.*

In this numerical experiment, the bicycle longitudinal velocity used for carrying out the numerical integration of the equations of motion employing the multibody computational procedure developed in this work is $v = 5$ (m/s). Consequently, being the radius of the rear wheel of the riderless bicycle equal to $R_r = 0.35$ (m), the angular velocity employed in the case of the bicycle system without the rider is $\omega = 15.29$ (rad/s).

It is important to note that, in the case of the nonlinear multibody model proposed in this paper for the Whipple-Carvallo bicycle system, the roll angular displacement denoted with ϕ and the steering angular displacement denoted with δ do not explicitly appear in the vector of generalized coordinates indicated with $\boldsymbol{q}$ that is used in the kinematic and dynamic descriptions of the bicycle multibody model. Consequently, in this general case, the roll and steering angles must be deduced through geometric considerations and by postprocessing the numerical results obtained from the nonlinear transient analysis. Thus, a general computational procedure described as follows is developed and used to solve this issue. First, two geometric vectors denoted with $\boldsymbol{v}_\alpha$ and $\boldsymbol{w}_\alpha$ associated with the two directions of interest are identified. The goal is to find the angle α defined between the two direction vectors $\boldsymbol{v}_\alpha$ and $\boldsymbol{w}_\alpha$. To this end, the next step is to calculate the scalar quantities indicated with x_α and y_α as follows:

$$\begin{cases} x_\alpha = \boldsymbol{v}_\alpha^T \boldsymbol{w}_\alpha \\ \\ y_\alpha = \|\boldsymbol{v}_\alpha \times \boldsymbol{w}_\alpha\| \end{cases} \tag{48}$$

Subsequently, the angle α of interest can be readily found by using the following equation:

$$\alpha = \text{atan2}(y_\alpha, x_\alpha) - \Gamma_\alpha \tag{49}$$

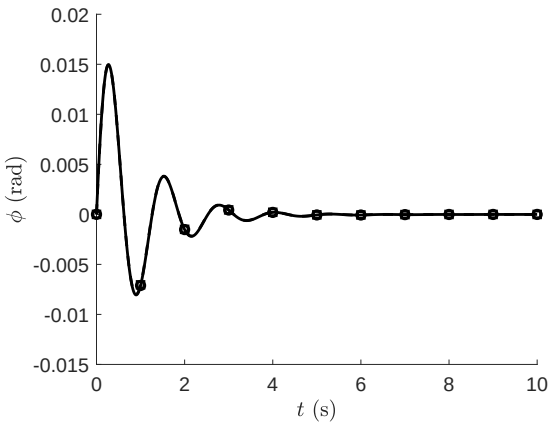

(a) *Roll angle obtained for an initial roll rate equal to* $\dot{\phi}_0 = 0.1$ *(rad/s) and using a longitudinal velocity equal to* $v = 5$ *(m/s).*

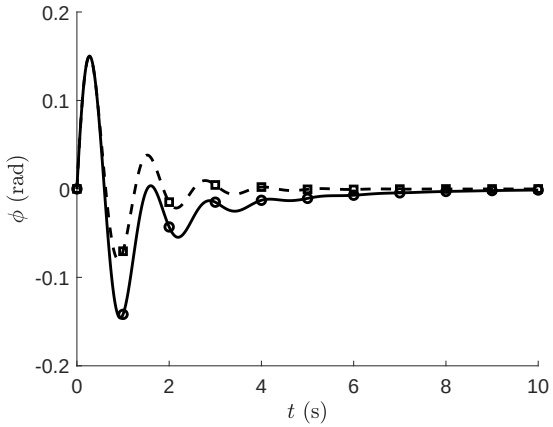

(b) *Roll angle obtained for an initial roll rate equal to* $\dot{\phi}_0 = 1.0$ *(rad/s) and using a longitudinal velocity equal to* $v = 5$ *(m/s).*

Figure 7. *Comparison of the dynamical behaviors of the linear and nonlinear riderless bicycle models resulting from a perturbation of the configuration of dynamic equilibrium: roll angular displacement of the proposed nonlinear riderless bicycle multibody model compared with the roll angle of the linear benchmark riderless bicycle model. The solid line (——) with circle markers* $(\circ)$ *represents the roll angle of the bicycle system calculated using the proposed nonlinear riderless multibody model. The dashed line (- - -) with square markers* $(\square)$ *represents the roll angle of the bicycle system calculated employing the linear benchmark riderless dynamic model.*

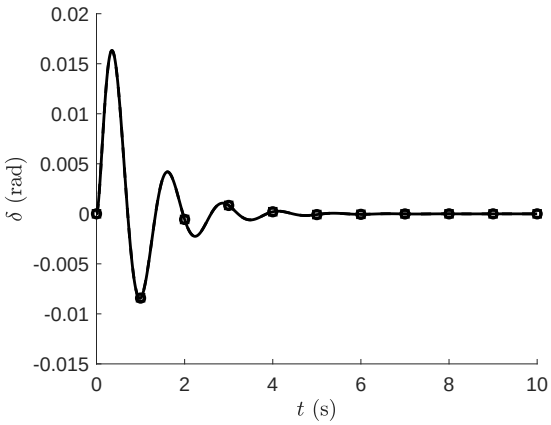

(a) *Steering angle obtained for an initial roll rate equal to* $\dot{\phi}_0 = 0.1$ *(rad/s) and using a longitudinal velocity equal to* $v = 5$ *(m/s).*

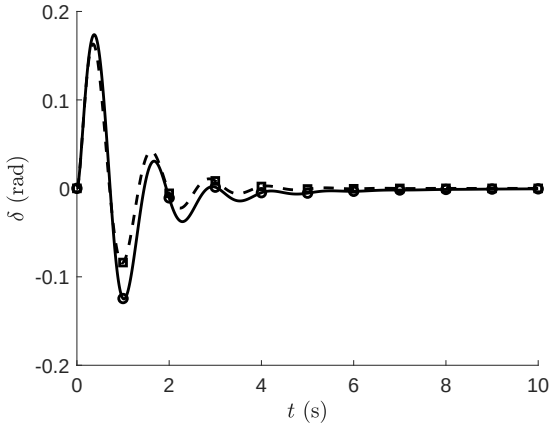

(b) *Steering angle obtained for an initial roll rate equal to* $\dot{\phi}_0 = 1.0$ *(rad/s) and using a longitudinal velocity equal to* $v = 5$ *(m/s).*

Figure 8. *Comparison of the dynamical behaviors of the linear and nonlinear riderless bicycle models resulting from a perturbation of the configuration of dynamic equilibrium: steering angular displacement of the proposed nonlinear riderless bicycle multibody model compared with the steering angle of the linear riderless benchmark bicycle model. The solid line (——) with circle markers* $(\circ)$ *represents the steering angle of the bicycle system calculated using the proposed nonlinear riderless multibody model. The dashed line (- - -) with square markers* $(\square)$ *represents the steering angle of the bicycle system calculated employing the linear benchmark riderless dynamic model.*

where Γ_α is a reference angle that serves to properly set to zero the reference value of the angle α under consideration. This simple computational procedure can be used to evaluate the roll angle ϕ and the steering angle δ starting from identifying two appropriate couples of direction vectors that define the geometric angles of interest. In particular, the roll angle ϕ of the bicycle system can be determined from the multibody model considering the following couple of direction vectors respectively denoted with $\boldsymbol{v}_\phi$ and $\boldsymbol{w}_\phi$, as well as by using the following reference angle denoted with Γ_ϕ:

$$\begin{cases} \boldsymbol{v}_\phi = \boldsymbol{k} \\ \\ \boldsymbol{w}_\phi = \boldsymbol{k}_1 \end{cases}, \quad \Gamma_\phi = \frac{\pi}{2} \tag{50}$$

where $\boldsymbol{k}$ is the unit vector associated with the axis Z of the global frame of reference and $\boldsymbol{k}_1$ is the unit vector corresponding to the axis $\bar{z}_1$ of the local reference system attached to the first body. These vectors are explicitly defined as follows:

$$\boldsymbol{k} = \begin{bmatrix} 0 & 0 & 1 \end{bmatrix}^T, \quad \begin{cases} \boldsymbol{k}_1 = \boldsymbol{A}_1 \bar{\boldsymbol{k}}_1 \\ \\ \bar{\boldsymbol{k}}_1 = \begin{bmatrix} 0 & 0 & 1 \end{bmatrix}^T \end{cases} \tag{51}$$

where $\boldsymbol{A}_1$ is the rotation matrix of the first body, namely the rear wheel. By observing the bicycle system from a front view in the plane OYZ, the roll angle ϕ is assumed to be positive when the bicycle rear wheel performs a counterclockwise rotation around the

X axis of the global reference system. Thus, the roll angle defined in the proposed multibody model has the same sign of those used in the benchmark bicycle models. Similarly, the steering angle δ of the bicycle system can be determined from the multibody model considering the following couple of direction vectors respectively denoted with $\boldsymbol{v}_\delta$ and $\boldsymbol{w}_\delta$, as well as by using the following reference angle denoted with Γ_δ:

$$\begin{cases} \boldsymbol{v}_\delta = \boldsymbol{k}_2 \\ \\ \boldsymbol{w}_\delta = \boldsymbol{j}_3 \end{cases}, \quad \Gamma_\delta = \frac{\pi}{2} \tag{52}$$

where $\boldsymbol{k}_2$ is the unit vector associated with the axis $\bar{z}_2$ of the local frame of reference attached to the second body and $\boldsymbol{j}_3$ is the unit vector corresponding to the axis $\bar{y}_3$ of the local reference system attached to the third body. These vectors are explicitly defined as follows:

$$\begin{cases} \boldsymbol{k}_2 = \boldsymbol{A}_2 \bar{\boldsymbol{k}}_2 \\ \\ \bar{\boldsymbol{k}}_2 = \begin{bmatrix} 0 & 0 & 1 \end{bmatrix}^T \end{cases}, \quad \begin{cases} \boldsymbol{j}_3 = \boldsymbol{A}_3 \bar{\boldsymbol{j}}_3 \\ \\ \bar{\boldsymbol{j}}_3 = \begin{bmatrix} 0 & 1 & 0 \end{bmatrix}^T \end{cases} \tag{53}$$

where $\boldsymbol{A}_2$ and $\boldsymbol{A}_3$ are the rotation matrices of respectively the second and third bodies, namely the rear frame and the front frame. By observing the bicycle system from a top view in the plane OXY, the steering angle δ is assumed to be positive when the bicycle front frame performs a counterclockwise rotation around an axis inclined of the caster angle with respect to the Z axis of the global reference system. Thus, the steering angle defined in the proposed multibody model has the opposite sign of those used in the benchmark bicycle models.

The computational procedure described above for the determination of the roll and steering angles allowed for performing a systematic comparison between the numerical results found employing the proposed nonlinear multibody model of the bicycle system and those deriving from the use of the benchmark models. As expected, although the entire set of numerical results found in the case of the proposed bicycle model is based on a nonlinear dynamical model, in the case of small perturbations, by observing Figures 5a, 6a, 7a, and 8a, the numerical results show only negligible differences between the time evolutions of the roll angle and steering angles of the proposed dynamical model compared with the same angles of the two benchmark models of the bicycle system. This is due to the hypothesis of small displacements assumed to linearize the proposed bicycle model for performing the stability study. On the other hand, when the magnitude of the perturbation imposed on the bicycle system increases, the hypothesis of linearity results is no longer valid for the linear benchmark model. Therefore, the use of the proposed nonlinear model becomes necessary. In this second case, in fact, the converse scenario is verified by means of a proper numerical analysis, as shown in Figures 5b, 6b, 7b, and 8b. Although the overall trend is identical for relatively large perturbations, the time histories of the roll and steering angles obtained by using the proposed nonlinear bicycle model differ from those arising from the use of the linear benchmark models. However, the numerical results found in both small and large perturbations are consistent with the physics of the problem under consideration.

3.4 Stability Influence Index

In this subsection, an influence index is introduced for establishing a quantitative metric for the analysis of bicycle stability. The goal is to understand which parameters have the greatest influence on the stability of the bicycle in the case of the straight motion. First, the most relevant model parameters of interest for the present analysis are identified in the comprehensive vector of physical parameters denoted with $\boldsymbol{b}$. This vector specifically defines the bicycle multibody model and includes geometric and inertial parameters, that are respectively grouped in the vectors $\boldsymbol{b}_g$ and $\boldsymbol{b}_i$ having dimensions $n_{b,g} = 6$ and $n_{b,i} = 40$, respectively, for a total of $n_b = 46$ model parameters. The subset of model parameters of interest is denoted with $\bar{\boldsymbol{b}}$ and includes both geometric and inertial quantities. In particular, the stability influence analysis is performed on a total of $\bar{n}_b = 28$ model parameters. In the subset of model parameters used for stability influence analysis, the geometric parameters considered include all the independent geometric quantities employed to define the system geometry. Thus, the subset of geometric parameters considered is denoted with $\bar{\boldsymbol{b}}_g$ and includes $\bar{n}_{b,g} = 6$ geometric quantities, that are the rear wheel radius denoted with R_r, the front wheel radius denoted with R_f, the wheelbase denoted with W_b, the fork offset denoted with H_f, the rear frame angle denoted with β, and the caster angle denoted with ε. Besides, the inertial parameters considered in the influence analysis are the most significant quantities that affect the dynamic behavior of the bicycle system. Therefore, the subset of inertial parameters considered is denoted with $\bar{\boldsymbol{b}}_i$ and includes $\bar{n}_{b,i} = 22$ inertial quantities that are the four nonzero horizontal and vertical positions of the centers of mass of the rear and front frame that are respectively denoted with $\bar{x}_{G_2}$, $\bar{z}_{G_2}$, $\bar{x}_{G_3}$, and $\bar{z}_{G_3}$, the four masses of the four rigid bodies of the model respectively denoted with m_1, m_2, m_3, and m_4, and the fourteen nonzero entries of the four inertia matrices of the rigid bodies that form the bicycle system respectively denoted with $\bar{\boldsymbol{I}}_{G_1}$, $\bar{\boldsymbol{I}}_{G_2}$, $\bar{\boldsymbol{I}}_{G_3}$, and $\bar{\boldsymbol{I}}_{G_4}$. In the present parametric analysis, reference is made to the numerical values of the physical parameters employed in the benchmark bicycle model with the rider described in detail in Table 3.

As discussed in the paper, the stability map of the Whipple-Carvallo bicycle system depends on the different values of the independent geometric and inertia parameters, which serve to describe the multibody model of the bicycle system. To understand how the specific values of the model parameters affect the stability of the bicycle system, an appropriate parametric analysis must be performed. To this end, a simple stability influence index, denoted with s_e, is properly defined and used to evaluate the influence of each parameter on the bicycle stability. Thus, this index specifies the impact that a given model parameter has on the amplitude of the stability region of the eigenvalues map of the bicycle multibody model. As already mentioned before in this work, the stability region of the Whipple-Carvallo bicycle system is delimited by two peculiar velocity values, namely the weave critical velocity denoted with $v_{w,c}$ and the capsize critical velocity denoted with $v_{c,c}$, which respectively identify the lower and upper limits of the stable region found in the bicycle stability map. Consequently, by varying the numerical values of the parameters embedded in the vectors $\bar{\boldsymbol{b}}_g$ and $\bar{\boldsymbol{b}}_i$, these peculiar critical velocity values can be calculated through numerical simulations for different model configurations to define the stability region in diverse cases.

Starting from the numerical values of the system parameters used in the benchmark bicycle model with the rider provided in Table 3, a scale factor κ is defined to facilitate the parametric analysis and to vary the values of the geometric and inertia parameters one by one. In each case, after the solution of the resulting generalized eigenvalue problem employed to obtain the stability map for the corresponding configuration of model parameters, the numerical values of the weave and capsize critical velocities can be readily identified. In particular, for a generic model parameter of the parameter vector $\bar{\boldsymbol{b}}$, the procedure mentioned before is structured as follows. For a given scale factor κ and starting from the value of the benchmark model with the rider, the stability map of the multibody model of the bicycle system can be derived in the different cases corresponding to the diverse values of the generic parameter $\bar{b}_h$, where h is an integer number that identifies the single entry $\bar{b}_h$ of the parameter vector $\bar{\boldsymbol{b}}$ of interest. The variation of

this parameter is computed as reported below:

$$\Delta\bar{b}_h = \kappa\bar{b}_h, \quad h = 1, 2, \ldots, \bar{n}_b \tag{54}$$

where κ is a real number used to vary the numerical value of the model parameter $\bar{b}_h$ and $\Delta\bar{b}_h$ represent the variation of the given model parameter. To achieve a meaningful parametric analysis, the value of κ is varied to obtain different plausible values of the selected parameter. This is done starting from the benchmark value, which corresponds to $\kappa = 1$, and by exploring a realistic range for the values of the geometric or inertial variable considered.

For each value of the varied generic model parameter, the corresponding critical velocities are calculated and stored into two velocity vectors, namely $\boldsymbol{v}_w$ and $\boldsymbol{v}_c$, that are respectively associated with the weave and capsize critical velocities found for the stability region in the eigenvalue map. In these vectors, the values of the critical velocities $v_{w,c}$ and $v_{c,c}$ obtained in the diverse cases corresponding to the variation of the specific model parameter of interest are respectively saved. Furthermore, for each model parameter examined, the difference between the two critical velocities identified at each step can be used as a discriminant to understand how much the parameter under investigation influences the amplitude of the stability region and the dynamics of the Whipple-Carvallo bicycle system in general. In fact, a large difference between the critical capsize velocity and the critical weave velocity is associated with a wider stability region. In contrast, a small difference between the two critical velocities characterizes a narrow stability zone. Therefore, it is apparent that, in the case in which one has a large stability region, the performance of the bicycle model is advantageous, and this scenario is preferable. Consequently, for a given model parameter, the ratio between the minimum and maximum values of the difference between the two critical velocities can be used as a valid numerical indicator of the significant variation of the stability region in the range of values considered for performing the parametric analysis.

For a specific model parameter $\bar{b}_h$, the following stability influence index indicated with s_e^h can be readily defined to obtain an appropriate number ranging between zero and one:

$$s_e^h = 1 - \frac{\min(\boldsymbol{v}_c^h - \boldsymbol{v}_w^h)}{\max(\boldsymbol{v}_c^h - \boldsymbol{v}_w^h)}, \quad h = 1, 2, \ldots, \bar{n}_b \tag{55}$$

where the vectors $\boldsymbol{v}_w^h$ and $\boldsymbol{v}_c^h$ respectively denote the vectors containing the weave and capsize critical velocities found on the stability map obtained by varying the parameter $\bar{b}_h$ and the integer number h represents the label of the specific parameter of interest that is varied during the parametric analysis. If there is a significant variation of the stability characteristics in the range explored for the model parameter, this fact is reflected in the difference between the capsize and weave critical velocities and the related maximum and minimum values of their differences. More precisely, an expansion of the stability region can be associated with a growth in the difference between the two critical velocities. Conversely, in the case of a contraction of the stability region, a relative decay of the difference between the critical velocities can be observed. Furthermore, if the parameter does not significantly affect the stability of the Whipple-Carvallo bicycle system, the stability region remains practically the same, and the difference between the critical velocities are almost constant for each varied value of the physical parameter chosen.

As a result of these observations, the stability influence index can be used to gain insights into the bicycle dynamical behavior and obtain quantitative information about the influence of the physical parameter examined on the stability of the bicycle multibody system running along a straight path with a constant forward velocity. In particular, for values of the stability influence index in the range $0.5 \leq s_e \leq 1$, the parameter has a high impact on the straight motion stability; for values of the stability influence index in the range $0.3 < s_e < 0.5$, the parameter has a medium effect on the straight motion stability; and for values of the stability influence index in the range $0 \leq s_e \leq 0.3$, the parameter has a low incidence on the straight motion stability of the Whipple-Carvallo bicycle system. To analyze the overall incidence of the $\bar{n}_b = 28$ parameters of interest for the stability analysis of the multibody model grouped in the vector $\bar{\boldsymbol{b}}$, the stability map was calculated for each variation $\Delta\bar{b}_h$ of the single parameter $\bar{b}_h$ under investigation. By doing so, about three thousand numerical simulations were carried out to obtain the comprehensive parametric analysis presented herein, and the numerical results found are summarized in Table 7.

In Table 7, the quantitative value of the stability influence index found for each relevant model parameter, and its corresponding qualitative weight, are reported. A close analysis of Table 7 reveals the relative level of influence on the bicycle stability of each relevant model parameter. In particular, one can observe that there are $\bar{n}_b^* = 6$ model parameters having a primary influence on bicycle stability. Basically, the parameters that have a major influence on the stability of the bicycle system are those related to the steering mechanism, namely the front frame and the front wheel, as well as to the rider, which is supposed to be rigidly attached to the rear frame and, therefore, its inertial effects are related to the second body of the multibody model. More specifically, the front wheel radius R_f, the fork offset H_f, the caster angle ε, and the third principal moment of inertia of the front wheel $I_{zz,4}$ define the geometric and inertial characteristics of the steering system, which plays a fundamental role in the dynamic behavior of a general two-wheeled vehicle. The inertial parameters of prime influence denoted with $\bar{x}_{G_2}$ and m_2, on the other hand, are respectively related to the horizontal position of the center of mass of the rear frame combined with the rider and to their total mass. In order to clarify this fundamental aspect, the model parameters having a high influence on the bicycle system stability are grouped in a parameter vector denoted with $\bar{\boldsymbol{b}}^*$. This important parameter vector is defined as follows:

$$\bar{\boldsymbol{b}}^* = \begin{bmatrix} R_f & \varepsilon & H_f & \bar{x}_{G_2} & I_{zz,4} & m_2 \end{bmatrix}^T \tag{56}$$

where the fundamental set of model parameters of primal influence is ordered following a descending order, from the most relevant parameter to the less relevant parameter, that is based on the values of their corresponding stability influence index found in the parametric analysis reported in Table 7. In the case of both the linear and nonlinear multibody models of the Whipple-Carvallo bicycle system, the subsequent dynamic analysis is, therefore, focused only on the impact of the six fundamental physical parameters of interest on the bicycle stability considering a straight motion with a constant longitudinal velocity.

3.5 Parametric Study of the Linear and Nonlinear Multibody Models

In this subsection, a parametric analysis is performed on the linear and nonlinear multibody models of the Whipple-Carvallo bicycle system to analyze the impact of the fundamental set of model parameters on the amplitude of the stability region, as well as their influence on the system nonlinear dynamic behavior. The set of six model parameters considered herein is identified through the stability analysis reported above in the manuscript. The main goal is to understand how the fundamental parameters of interest influence the stability of the bicycle straight motion considering both the linear and nonlinear multibody models.

The first part of this subsection is concerned with describing the numerical results relative to the parametric analysis performed in the case of the linear multibody model of the bicycle system. To this end, in the case of the linear bicycle model developed in this work, the effects on the stability of the parameters classified with great influence are represented in Figure 9.

In Figure 9, the variation of the weave and capsize critical velocities is shown in correspondence of a small variation in a realistic range of each model parameter of primary relevance. In particular, Figures 9a, 9b, 9c, 9d, 9e, and 9f represent the graphical results of

Table 7. Quantitative and qualitative influence on the bicycle stability of each relevant parameter of the multibody model.

Model Parameter	Stability Influence Index	Low Influence	Medium Influence	High Influence
R_r	0.1327	√		
R_f	0.9424			√
W_b	0.4979		√	
H_f	0.7659			√
β	0.2167	√		
ε	0.8712			√
$\bar{x}_{G_2}$	0.7527			√
$\bar{z}_{G_2}$	0.3320		√	
$\bar{x}_{G_3}$	0.2644	√		
$\bar{z}_{G_3}$	0.2657	√		
m_1	0.0281	√		
m_2	0.5039			√
m_3	0.2536		√	
m_4	0.3224		√	
$I_{xx,1}$	0.0056	√		
$I_{yy,1}$	0.0056	√		
$I_{zz,1}$	0.2150	√		
$I_{xx,2}$	0.3627		√	
$I_{yy,2}$	0.3439		√	
$I_{zz,2}$	0	√		
$I_{xy,2}$	0.4056		√	
$I_{xx,3}$	0.0225	√		
$I_{yy,3}$	0.0056	√		
$I_{zz,3}$	0	√		
$I_{xy,3}$	0.0112	√		
$I_{xx,4}$	0.3568		√	
$I_{yy,4}$	0.3568		√	
$I_{zz,4}$	0.7117			√

the parametric analysis performed on the weave and capsize critical velocities in the case of the variation of the front wheel radius R_f, the caster angle ε, the fork offset H_f, the abscissa of the rear frame center of mass $\bar{x}_{G_2}$, the third mass moment of inertia of the front wheel $I_{zz,4}$, and the mass of the rear frame m_2, respectively. In the case of the linear multibody model of the Whipple-Carvallo bicycle system, by analyzing the general parametric study synthetically represented in Figure 9, one can observe that a significant enlargement of the bicycle stability region can be obtained by increasing the numerical values used for the front wheel radius R_f and the caster angle ε. Furthermore, by increasing the horizontal position of the rear frame centroid $\bar{x}_{G_2}$ and the mass of the rear frame m_2, a moderate extension of the amplitude of the bicycle stability region can be obtained as well. On the other hand, by decreasing the length of the fork offset H_f and the magnitude of the third principal mass moment of inertia of the front wheel $I_{zz,4}$, one can still obtain a relatively important enlargement of the stability region. This qualitative behavior is consistent with the physics of the bicycle system and agrees with what is found in the literature [25–27].

The second part of this subsection deals with the discussion of the numerical results of the parametric analysis found in the case of the nonlinear multibody model of the bicycle system. Thereby, the proposed bicycle multibody model can be used for performing numerical experiments with high confidence to explore dynamical scenarios that are not fully captured by the benchmark model of the Whipple-Carvallo bicycle system. As discussed in this section, the dynamic behavior of the Whipple-Carvallo bicycle system is strictly correlated to the geometry of the vehicle as well as to its inertial properties. Therefore, the nonlinear multibody model can be effectively employed to show the difference in the dynamical response of the bicycle system for the same operating conditions and varying the fundamental geometric and inertial parameters already analyzed using the linearized model. For this purpose, in the case of the nonlinear bicycle model devised in this paper, the numerical results of this second analysis devoted to investigating the impact of the parameters recognized as more significant are respectively represented in Figures 10, 11, 12, 13, 14, and 15.

All the dynamical simulations were performed considering a fixed longitudinal velocity of the bicycle equal to $v = 5.5$ (m/s) and by imposing as an external perturbation an initial roll rate equal to $\dot{\phi}_0 = 0.5$ (rad/s). Figures 10a and 10b respectively represent the graphical results of the parametric analysis for the roll and steering angular displacements of the nonlinear multibody model of the bicycle system obtained in the case of the variation of the front wheel radius R_f for three typical values that are respectively equal to $R_f = 0.3$ (m), $R_f = 0.35$ (m), and $R_f = 0.45$ (m). Figures 11a and 11b respectively represent the graphical results of the parametric analysis for the roll and steering angular displacements of the nonlinear multibody model of the bicycle system obtained in the case of the variation of the caster angle ε for three typical values that are respectively equal to $\varepsilon = 0.157$ (rad), $\varepsilon = 0.314$ (rad), and $\varepsilon = 0.628$ (rad). Figures 12a and 12b respectively represent the graphical results of the parametric analysis for the roll and steering angular displacements of the nonlinear multibody model of the bicycle system obtained in the case of the variation of the fork offset H_f for three typical values that are respectively equal to $H_f = 0.0160$ (m), $H_f = 0.0321$ (m), and $H_f = 0.0641$ (m). Figures 13a and 13b respectively represent the graphical results of the parametric analysis for the roll and steering angular displacements of the nonlinear multibody model of the bicycle system obtained in the case of the variation of the rear frame centroid abscissa $\bar{x}_{G_2}$ for three typical values that are respectively equal to $\bar{x}_{G_2} = 0.15$ (m), $\bar{x}_{G_2} = 0.3$ (m), and $\bar{x}_{G_2} = 0.45$ (m). Figures 14a and 14b respectively represent the graphical results of the parametric analysis for the roll and steering angular displacements of the nonlinear multibody model of the bicycle system obtained in the case of the variation of the front wheel inertia moment $I_{zz,4}$ for three typical values that are respectively equal to $I_{zz,4} = 0.224$ (kg×m^2), $I_{zz,4} = 0.28$ (kg×m^2), and $I_{zz,4} = 0.42$ (kg×m^2). Figures

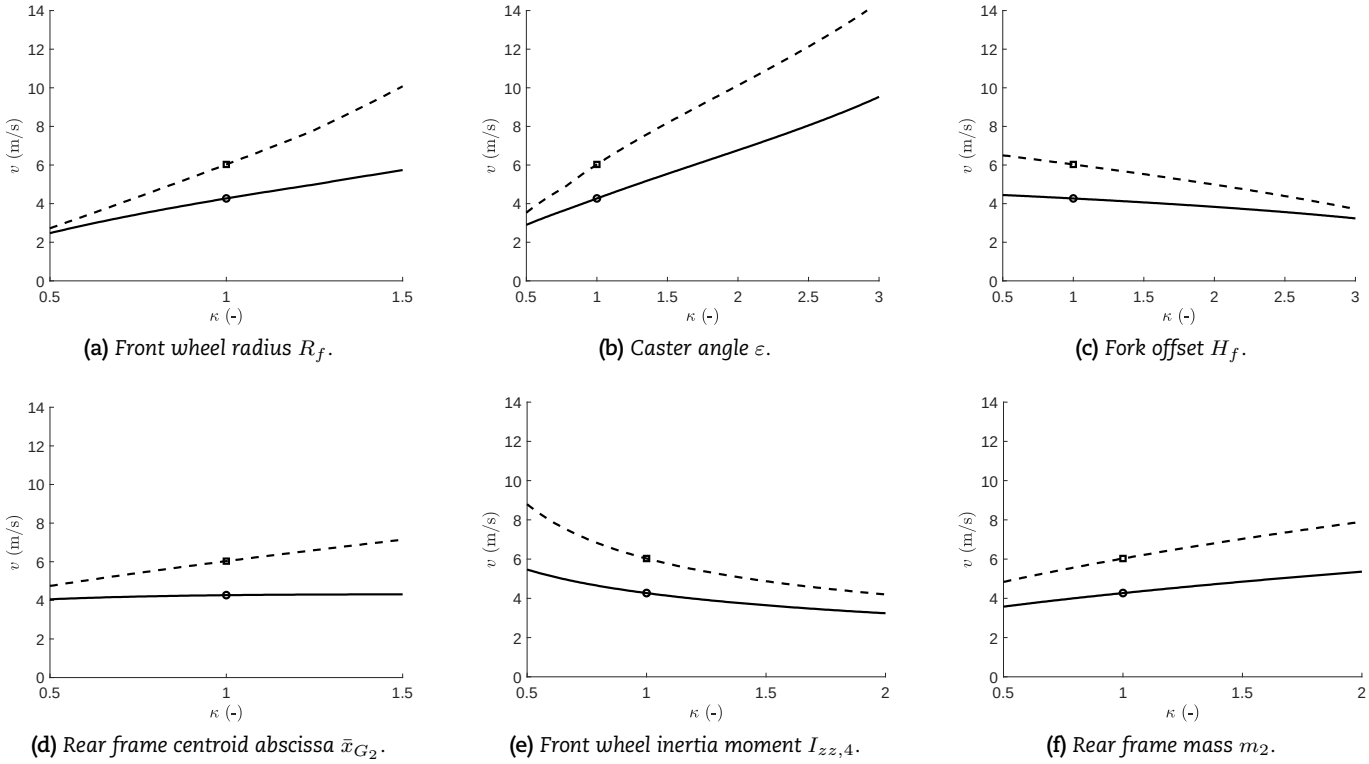

(a) *Front wheel radius* R_f. **(b)** *Caster angle* ε. **(c)** *Fork offset* H_f.

(d) *Rear frame centroid abscissa* $\bar{x}_{G_2}$. **(e)** *Front wheel inertia moment* $I_{zz,4}$. **(f)** *Rear frame mass* m_2.

Figure 9. *Influence of the fundamental system parameters on the bicycle stability region in the case of the linear multibody model. The solid line (——) represents the weave critical velocity* $v_{c,w}$*, the circle marker* $(\circ)$ *indicates the benchmark value of the weave critical velocity, the dashed line (- - -) represents the capsize critical velocity* $v_{c,c}$*, the square marker* $(\square)$ *indicates the benchmark value of the capsize critical velocity. The parameter* κ *is the proportional factor used to vary the numerical values of the model parameters of interest. For* $\kappa = 1$*, the parameters are all equal to the benchmark values relative to the bicycle system with the rider.*

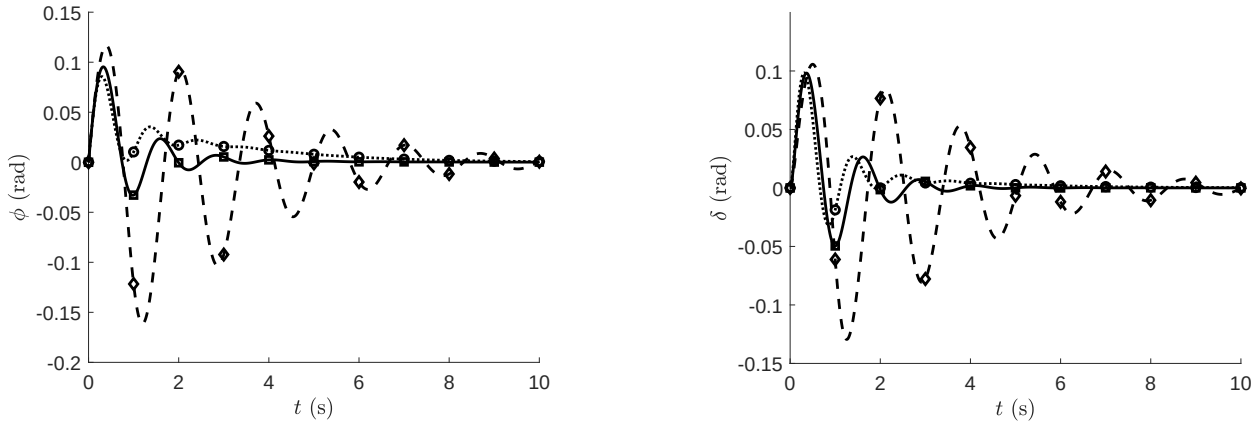

(a) *Roll angle obtained for an initial roll rate equal to* $\dot{\phi}_0 = 0.5$ *(rad/s) and using a longitudinal velocity equal to* $v = 5.5$ *(m/s).*

(b) *Steering angle obtained for an initial roll rate equal to* $\dot{\phi}_0 = 0.5$ *(rad/s) and using a longitudinal velocity equal to* $v = 5.5$ *(m/s).*

Figure 10. *Comparison of the roll angular displacement and the steering angular displacement of the nonlinear bicycle models with the rider obtained for different values of the front wheel radius. The solid lines (——) with the square markers* $(\square)$ *represent the roll angle and the steering angle obtained for a front wheel radius equal to the benchmark value* $R_f = 0.35$ *(m). The dotted lines (·····) with circle markers* $(\circ)$ *represent the roll angle and the steering angle obtained for a front wheel radius equal to* $R_f = 0.3$ *(m). The dashed lines (- - -) with the diamond markers* $(\diamond)$ *represent the roll angle and the steering angle obtained for a front wheel radius equal to* $R_f = 0.45$ *(m).*

15a and 15b respectively represent the graphical results of the parametric analysis for the roll and steering angular displacements of the nonlinear multibody model of the bicycle system obtained in the case of the variation of the rear frame mass m_2 for three typical values that are respectively equal to $m_2 = 75$ (kg), $m_2 = 85$ (kg), and $m_2 = 95$ (kg).

In general, as shown in Figures 10, 11, 12, 13, 14, and 15, an increase in one of the six parameters of interest is mainly associated with an augmentation of the importance of the nonlinear phenomena. This reflects on an appreciable qualitative change of the time evolution of the bicycle roll and steering angular displacements in terms of their general trend and their vibration amplitudes. In fact, regarding the incidence of the various parameters on the bicycle stability, rather than making an absolute analysis on the value of the particular parameter, this problem should be studied considering the numerical value of the longitudinal velocity employed in the analysis and the relative width of the stability zone. In practice, with the same longitudinal velocity, the process of changing

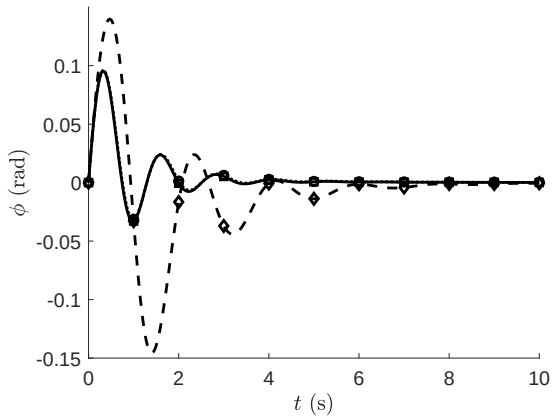

(a) *Roll angle obtained for an initial roll rate equal to* $\dot{\phi}_0 = 0.5$ *(rad/s) and using a longitudinal velocity equal to* $v = 5.5$ *(m/s).*

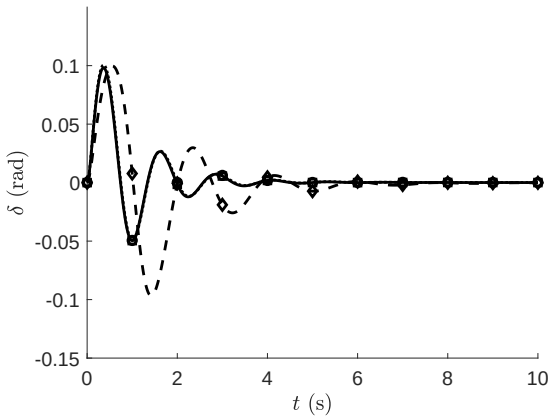

(b) *Steering angle obtained for an initial roll rate equal to* $\dot{\phi}_0 = 0.5$ *(rad/s) and using a longitudinal velocity equal to* $v = 5.5$ *(m/s).*

Figure 11. *Comparison of the roll angular displacement and the steering angular displacement of the nonlinear bicycle models with the rider obtained for different values of the caster angle. The solid lines (——) with the square markers* (□) *represent the roll angle and the steering angle obtained for a caster angle equal to the benchmark value* $\varepsilon = 0.314$ *(rad). The dotted lines (·····) with circle markers* (○) *represent the roll angle and the steering angle obtained for a caster angle equal to* $\varepsilon = 0.157$ *(rad). The dashed lines (- - -) with the diamond markers* (◇) *represent the roll angle and the steering angle obtained for a caster angle equal to* $\varepsilon = 0.628$ *(rad).*

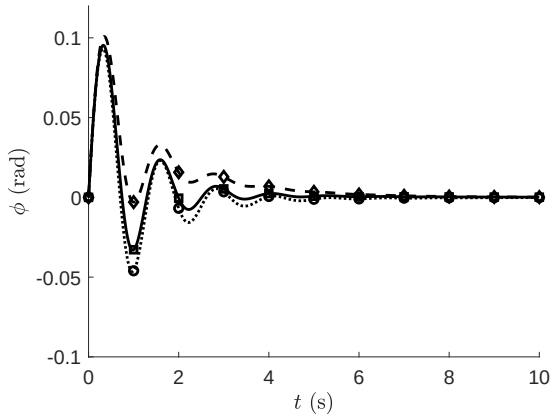

(a) *Roll angle obtained for an initial roll rate equal to* $\dot{\phi}_0 = 0.5$ *(rad/s) and using a longitudinal velocity equal to* $v = 5.5$ *(m/s).*

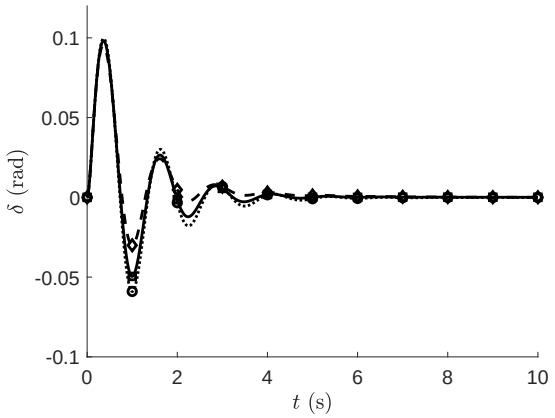

(b) *Steering angle obtained for an initial roll rate equal to* $\dot{\phi}_0 = 0.5$ *(rad/s) and using a longitudinal velocity equal to* $v = 5.5$ *(m/s).*

Figure 12. *Comparison of the roll angular displacement and the steering angular displacement of the nonlinear bicycle models with the rider obtained for different values of the fork offset. The solid lines (——) with the square markers* (□) *represent the roll angle and the steering angle obtained for a fork offset equal to the benchmark value* $H_f = 0.0321$ *(m). The dotted lines (·····) with circle markers* (○) *represent the roll angle and the steering angle obtained for a fork offset equal to* $H_f = 0.0160$ *(m). The dashed lines (- - -) with the diamond markers* (◇) *represent the roll angle and the steering angle obtained for a fork offset equal to* $H_f = 0.0641$ *(m).*

the numerical value of the geometric or inertial parameter of interest can lead the system behavior closer to the upper or the lower limit of the stability zone. Consequently, the resulting stability behavior is necessarily different. Since, in that case, the stability zone has changed, because of the variation of a geometric or inertial parameter, the bicycle system turns out to be in a different point of the stability zone and, therefore, its dynamical behavior is different. As a result, the nonlinear analysis allows for capturing this crucial aspect more directly than by simply evaluating the eigenvalues represented on the stability map, obtained through the linear analysis carried out at a given forward velocity and for a given set of geometric and inertial parameters. Thus, the combined effect of the system geometry variation, the forward velocity, and the external perturbation should always be considered to examine the resulting system dynamical behavior properly. To this end, the proposed multibody approach, which leverages both linear and nonlinear parametric analysis, can be helpful in simplifying the complex problem represented by the bicycle dynamics.

3.6 Discussion and Final Remarks

In this subsection, a comprehensive discussion on the numerical results found in the paper by using the analytical approach presented in this two-part manuscript is provided, together with some final remarks on the stability analysis of the straight motion of the Whipple-Carvallo bicycle system, obtained employing the linear and nonlinear multibody models developed in this work.

First, to perform a consistent comparison with the numerical results found in the literature, the process of obtaining from the benchmark bicycle models the suitable numerical values of the system parameters to be used in the computer implementation of the bicycle multibody model of interest for this paper was carried out. By using a systematic approach to derive the linearized dynamic equations from the nonlinear model obtained with the use of the D'Alambert-Lagrange equations of motion, the numerical results found employing the benchmark numerical values for the system parameters were compared with those of the benchmark model concerning the linear stability analysis of the motion of the bicycle system along a straight line. With this respect, Tables 3 and 4 respectively contain the benchmark data conversion in the case of the Whipple-Carvallo bicycle system with and without

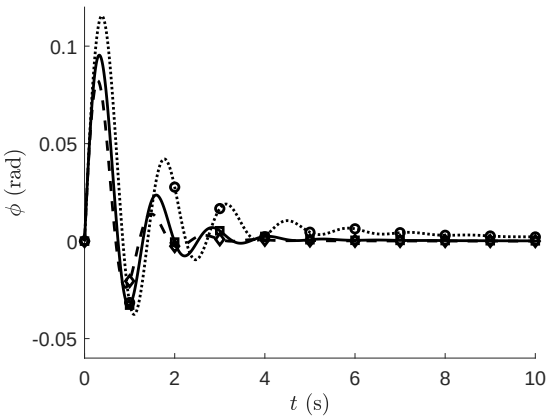

(a) *Roll angle obtained for an initial roll rate equal to* $\dot{\phi}_0 = 0.5$ *(rad/s) and using a longitudinal velocity equal to* $v = 5.5$ *(m/s).*

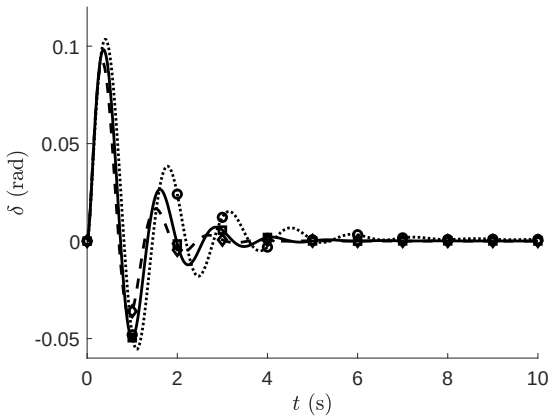

(b) *Steering angle obtained for an initial roll rate equal to* $\dot{\phi}_0 = 0.5$ *(rad/s) and using a longitudinal velocity equal to* $v = 5.5$ *(m/s).*

Figure 13. *Comparison of the roll angular displacement and the steering angular displacement of the nonlinear bicycle models with the rider obtained for different values of the rear frame centroid abscissa. The solid lines (——) with the square markers* (□) *represent the roll angle and the steering angle obtained for a rear frame centroid abscissa equal to the benchmark value* $\bar{x}_{G_2} = 0.3$ *(m). The dotted lines (·····) with circle markers* (○) *represent the roll angle and the steering angle obtained for a rear frame centroid abscissa equal to* $\bar{x}_{G_2} = 0.15$ *(m). The dashed lines (- - -) with the diamond markers* (◇) *represent the roll angle and the steering angle obtained for a rear frame centroid abscissa equal to* $\bar{x}_{G_2} = 0.45$ *(m).*

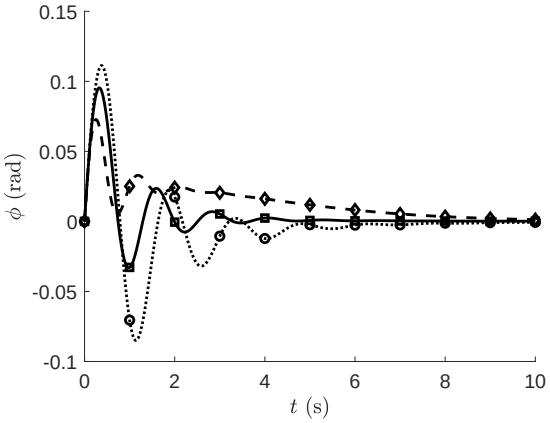

(a) *Roll angle obtained for an initial roll rate equal to* $\dot{\phi}_0 = 0.5$ *(rad/s) and using a longitudinal velocity equal to* $v = 5.5$ *(m/s).*

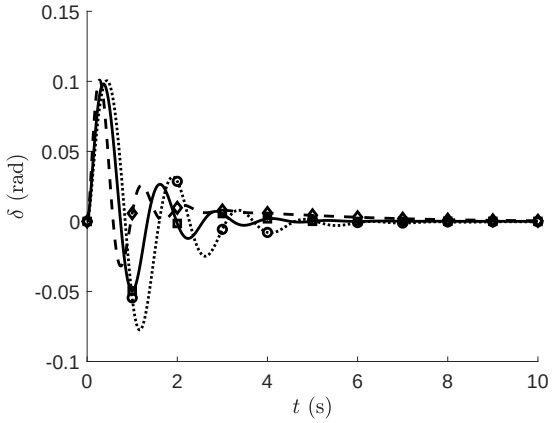

(b) *Steering angle obtained for an initial roll rate equal to* $\dot{\phi}_0 = 0.5$ *(rad/s) and using a longitudinal velocity equal to* $v = 5.5$ *(m/s).*

Figure 14. *Comparison of the roll angular displacement and the steering angular displacement of the nonlinear bicycle models with the rider obtained for different values of the front wheel inertia moment. The solid lines (——) with the square markers* (□) *represent the roll angle and the steering angle obtained for a front wheel inertia moment equal to the benchmark value* $I_{zz,4} = 0.28$ $(\mathrm{kg}\times\mathrm{m}^2)$*. The dotted lines (·····) with circle markers* (○) *represent the roll angle and the steering angle obtained for a front wheel inertia moment equal to* $I_{zz,4} = 0.224$ $(\mathrm{kg}\times\mathrm{m}^2)$*. The dashed lines (- - -) with the diamond markers* (◇) *represent the roll angle and the steering angle obtained for a front wheel inertia moment equal to* $I_{zz,4} = 0.42$ $(\mathrm{kg}\times\mathrm{m}^2)$*.*

the rider. Thus, the graphic representation of the eigenvalues represented in Figures 3 and 4 show a perfect agreement between the linearization of the proposed multibody model and the benchmark bicycle models. This qualitative observation is confirmed by the quantitative results reported in Tables 5 and 6, which show that the small differences in the numerical results are only due to the computation accuracy of the computer calculations.

Subsequently, a nonlinear stability analysis was performed considering the proposed bicycle multibody model and through the use of the constraint stabilization algorithm devised in this paper for nonholonomic multibody systems. To this end, the numerical results found were compared with those obtained from the benchmark bicycle system with and without the rider. This comparative analysis aimed to compare the numerical solutions of the linear benchmark model and the nonlinear model developed by the authors in response to the same external perturbation. For this purpose, a general and effective method for constructing the bicycle roll and steering angular displacements from the generalized coordinate vector of the detailed multibody model was developed and used to compare with the linear benchmark models.

For the bicycle with the rider and the riderless bicycle model, a systematic comparison was performed considering the proposed nonlinear multibody model and the linear benchmark models in the case of a small perturbation from the configuration of dynamic equilibrium. Figures 5a and 6a refer to the resulting roll and steering angular displacements of the bicycle in the case of a small perturbation of the model with the rider. Figures 7a and 8a refer to the resulting roll and steering angular displacements of the bicycle in the case of a small perturbation of the model without the rider. These figures show that the numerical results are practically equivalent since the perturbation is small. On the other hand, in the case of a large perturbation from the configuration of dynamic equilibrium, the bicycle with the rider and the riderless bicycle model were analyzed. A comprehensive comparison was carried

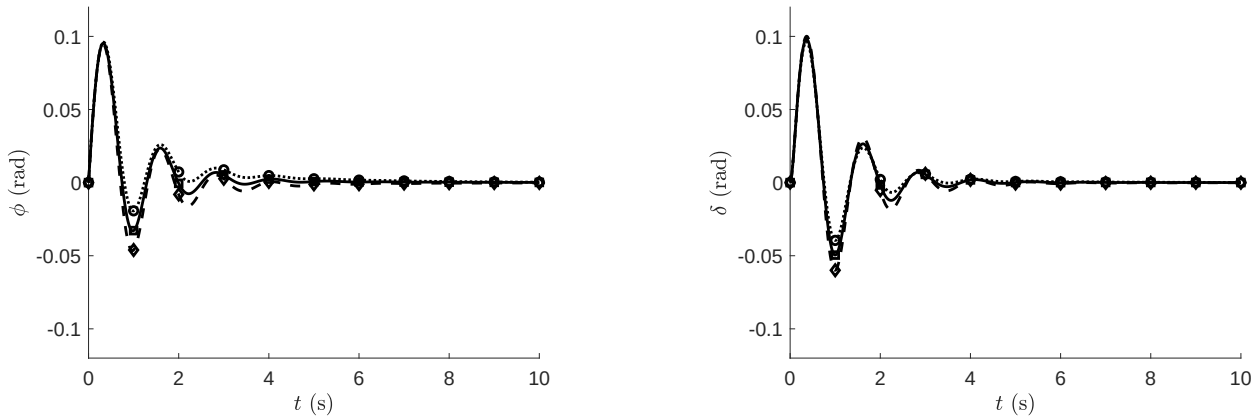

(a) *Roll angle obtained for an initial roll rate equal to* $\dot{\phi}_0 = 0.5$ *(rad/s) and using a longitudinal velocity equal to* $v = 5.5$ *(m/s).*

(b) *Steering angle obtained for an initial roll rate equal to* $\dot{\phi}_0 = 0.5$ *(rad/s) and using a longitudinal velocity equal to* $v = 5.5$ *(m/s).*

Figure 15. *Comparison of the roll angular displacement and the steering angular displacement of the nonlinear bicycle models with the rider obtained for different values of the rear frame mass. The solid lines (——) with the square markers* (□) *represent the roll angle and the steering angle obtained for a rear frame mass equal to the benchmark value* $m_2 = 85$ *(kg). The dotted lines (·····) with circle markers* (○) *represent the roll angle and the steering angle obtained for a rear frame mass equal to* $m_2 = 75$ *(kg). The dashed lines (- - -) with the diamond markers* (◇) *represent the roll angle and the steering angle obtained for a rear frame mass equal to* $m_2 = 95$ *(kg).*

out considering the proposed nonlinear multibody model and the linear benchmark models. To this end, Figures 5b and 6b refer to the resulting roll and steering angular displacements of the bicycle in the case of a large perturbation of the model with the rider. Figures 7b and 8b refer to the resulting roll and steering angular displacements of the bicycle in the case of a large perturbation of the model without the rider. Thus, for a relatively larger disturbance, the numerical results of the proposed bicycle multibody model start to diverge from those arising from the linear benchmark models, pointing out the necessity to use a nonlinear model to study the complex dynamical behavior of the bicycle system. This behavior is the necessary consequence of large displacements and finite rotations of a complex articulated mechanical system such as the bicycle system, which are more properly described by nonlinear differential-algebraic equations of motion rather than linear ordinary differential dynamic equations.

Afterward, an appropriate performance index was introduced and used as a quantitative metric to assess the stability of the bicycle system in the case of a straight motion. By doing so, a reduced set of parameters having the greatest impact on the stability of the bicycle system was identified. As reported in Table 7, some model parameters affect more than others the bicycle stability during a straight motion, leading to the identification of a set of six fundamental model parameters. As a general rule, to a higher value of the stability influence index denoted with s_e^h, that corresponds to the general parameter labeled with the integer number h, a greater influence on the dynamical properties of the bicycle is associated. As shown by the numerical results reported in Table 7, the set of model parameters having a primary influence on the stability of the bicycle system is composed of six geometric and inertial parameters. These fundamental parameters, ordered from the most influential parameter to the last influential parameter, are the front wheel radius R_f, the caster angle ε, the fork offset H_f, the horizontal position of the center of mass of the rear frame $\bar{x}_{G_2}$, the third principal moment of inertia of the front wheel $I_{zz,4}$, and the mass of the rear frame m_2.

Finally, considering both the linear and nonlinear multibody models of the Whipple-Carvallo bicycle system, a comprehensive parametric study was carried out. The parametric study aimed to analyze the influence of the fundamental set of model parameters on the dimension of the stability region and their impact on the nonlinear dynamic behavior of the bicycle system. This study represents the core part of the numerical results obtained in this investigation, discussed and commented on below. First, a parametric analysis of the linear multibody model was performed, leading to the numerical results represented in Figure 9. A consequential analysis was then carried out employing the nonlinear model to capture the nonlinear effect induced by the variation of one of the fundamental geometric and inertial parameters on the bicycle stability, explored using the linearized multibody model. The numerical results of this second parametric analysis are represented in Figures 10, 11, 12, 13, 14, and 15.

In Figures 9a and 9b, the effects of the front wheel radius R_f and of the variation of the caster angle ε on the bicycle stability are respectively shown. In both cases, an increment of R_f or ε results in the growth of both the capsize and weave critical velocities. On the other hand, as shown in Figure 9c, an increment of the fork offset H_f results in a lower value for both the critical velocities. The qualitative variations of the stability region, as well as the quantitative dynamical behavior resulting from the numerical results found by using the bicycle multibody model developed in this paper, are in agreement with the general considerations and the conclusive remarks of other authors, such as Cossalter [24] and Franke et al. [27]. In fact, in [24], the author comments as follows: 'long trails assures a high directional stability'. Also, in [27], the authors wrote the following remark: 'the stability region grows linearly with the trail while it tends to large velocities'. This is also consistent with the behavior of the linear benchmark model of the Whipple-Carvallo bicycle system proposed by Meijaard et al. in [4] and by Kooijman et al. in [5]. As can be seen from Equation (14), the geometric trail T_b depends on the front wheel radius R_f, on the fork offset H_f, and on the caster angle ε. Therefore, the nonlinear bicycle model proposed in this paper behaves following the previous considerations because the geometric trail grows with the caster angle ε and with the front wheel radius R_f. At the same time, it diminishes with the fork offset H_f.

In Figures 9d and 9f, the effect of the center of mass horizontal position and the influence of the mass of the rear frame are respectively represented. In particular, in Figure 9f, one can observe how the rear frame mass influences the stability region. Indeed, for a smaller value of the rear frame mass, which can be seen as a lighter rider, the zone of stability moves to smaller velocities values. This indicates that the rider is responsible for the stability characteristics of the whole rider-bicycle system. Furthermore, another important aspect related to the influence of the rider was already pointed out by Franke et al. in [27], who stated that: 'shifting the position of the rider forward causes a similar effect to that caused by lengthening the trail'. As shown in Figure 9d, this phenomenon is confirmed by the numerical results obtained from the parametric analysis performed in this paper. In Figure 9e, the effect of the third principal moment of inertia of the front wheel around the axis of rotation shows that, for higher values of this moment of inertia, the stability region moves forward, thereby corresponding to higher values of the critical velocity, but, at the same time, it becomes smaller. This behavior is also found in the previous investigations reported in the literature [24, 27].

As far as the nonlinear phenomena are concerned, the effects of the geometric and inertia properties of the Whipple-Carvallo bicycle system were analyzed using the nonlinear multibody model developed by the authors. To this end, by exploring a variation of the six fundamental parameters of interest, some significant information can be gathered from the evolution in time of the roll angle ϕ and of the steering angle δ. In this case, the set of numerical results found in correspondence of the variation of each model parameter of interest are respectively represented in Figures 10, 11, 12, 13, 14, and 15. As shown in these figures, a significant variation of one of the six parameters of interest is mainly associated with an augmentation of the importance of the nonlinear phenomena. More specifically, the bicycle system exhibits a damped behavior in the limit of the stability zone, even though no dissipation is explicitly considered in the nonlinear multibody model. This property is peculiar to nonholonomic systems, and it is strictly connected to the modeling of the contact between the wheels and the ground. For this purpose, the contact was modeled in this investigation using an appropriate set of nonholonomic constraints representing the pure rolling condition, leading to the peculiar nonlinear behavior observed in the dynamical simulations.

Observing the nonlinear behavior of the bicycle system consequent to an external perturbation, both the roll angle and the steering angle oscillate around the configuration of dynamic equilibrium with an amplitude depending on the geometric and inertial characteristics of the bicycle system, as well as on the magnitude of the external disturbance. Furthermore, the amplitudes of the nonlinear vibrations represented in Figures 10, 11, 12, 13, 14, and 15 demonstrate the importance of the design process devoted to properly tune the system parameters to obtain a dynamical behavior consistent with the desired performance. For the same external perturbation, in a small range of longitudinal velocities, the dynamical response of the model around the equilibrium configuration is not as negligible as one could expect. Namely, the nonlinear oscillation of the system around the configuration of dynamic equilibrium depends on the bicycle forward velocity, resulting in smaller amplitudes for higher velocities and in what can be defined as a more stable dynamic behavior. By observing the physical behavior of the bicycle system, these numerical results can also be confirmed by practical experiments, where the bicycle tends to respond better to little impulses at higher velocities than at lower ones [38].

For all the reasons mentioned above, the restricted set of model parameters identified in this investigation employing numerical experiments must be carefully designed. A particular combination of them will result in a specific stability region that can be suited or not for the specific application considered. Therefore, by constructing an accurate virtual prototype based on the proposed multibody approach to the dynamics of articulated mechanical systems, one can understand how to address the design of the different parts of the bicycle system, thereby attaining a realistic prediction of the performance of the actual final result. To achieve this goal, the analytical and numerical methodologies devised in this investigation, as well as the systematic parametric analysis proposed in this work, can be successfully employed.

4. Summary, Conclusions, and Future Work

This paper fits an extended research plan devoted to analyzing multibody systems [65,66], the design of nonlinear control laws for dynamical systems [67,68], and identifying the dynamical model of mechanical systems [69,70]. In particular, in this investigation, a general multibody approach is employed for analyzing bicycle systems and the Whipple-Carvallo bicycle model is considered as the case study. For this purpose, this manuscript is the second contribution of a two-part research paper.

In this investigation, the system of differential-algebraic equations describing the motion of the Whipple-Carvallo bicycle model of interest is obtained using the D'Alambert-Lagrange principle of virtual work with the analytical technique of the Lagrange multipliers. By employing a systematic procedure that is well suited for computer implementation, the equations are then linearized and are further used to obtain different information on the dynamic behavior of the bicycle system. Before the implementation of the alternative linearization technique and the constraint stabilization method shown in the first part of this two-part paper, in the second part of this two-part investigation, the symbolic form of the equations of motion of the bicycle model is obtained and transformed into a set of numerical subroutines through the use of a general-purpose multibody code developed by the authors in MATLAB. This approach allows for controlling the most relevant aspects of the multibody model and defining the geometry of the system in a parametric way for quickly analyzing the effects of the most critical geometric quantities on the dynamical behavior of the vehicle and its stability characteristics. By doing so, an extensive parametric analysis based on the linearized and nonlinear bicycle models is carried out to individuate the most significant parameters influencing the stability characteristics of the bicycle system and, subsequently, their dynamical effects are quantified by exploring a realistic range of variation. A proper combination of the numerical values of those geometric and inertial parameters defines a specific dynamical behavior of the bicycle system, which can be changed and eventually tuned according to the desired performance. The analytical approach and the computational algorithm presented in this two-part investigation are general and are based on a systematic multibody approach that can be applied to different mechanical systems with high confidence since the numerical results obtained in this second research work are in perfect agreement with the benchmark results presented in the literature. Moreover, since it is based on a fully nonlinear description, the proposed methodology allowed for analyzing engaging scenarios not covered in other previous research works.

This paper presents a bicycle multibody model that can be used to perform preliminary parametric analysis to help the designing process and understand with a relatively small effort how the different geometric and inertial parameters of the system affect its straight motion stability. To verify the numerical results obtained in the paper, the developed model is initially used to reproduce the results of the bicycle benchmark model described by Meijaard et al. in [4] and, subsequently, the results of the riderless bicycle benchmark model described by Kooijman et al. in [5]. After that, the results of the nonlinear model developed by the authors and the linear benchmark models show the difference that arises using a linearized model and the original nonlinear one. Finally, the comparison of the numerical results of the linear and nonlinear parametric analysis developed considering the bicycle multibody model devised in the paper is presented. To this end, considering a parametric description of the physical system of interest, the resulting mathematical model can be used to perform comprehensive nonlinear and linear analysis based on an analytical formulation and a computational strategy both well suited for the computer-aided numerical implementation. Employing the approach presented in this paper, it is possible to obtain a proper mathematical model of a general multibody system consistent with the physics of the problem. By doing so, the comprehensive multibody model of the Whipple-Carvallo bicycle model investigated in this paper can be used to identify and evaluate the effects of the more relevant geometric and inertial parameters that influence the dynamics of the system of interest, as well as to analyze the complete nonlinear model of a general bicycle system and its linearized counterpart to make comparisons with different studies found in the literature.

As discussed in detail in the paper, the proposed multibody model undoubtedly represents a mathematical abstraction of the physical bicycle system. In this respect, although the nonlinearities in the proposed multibody model allow for correctly capturing the peculiar geometric features of the bicycle system and its resulting self-balancing dynamical behavior, there are at least three main limitations of the proposed bicycle model that should be eventually removed in the future investigations. These are the use of ideal rigid bodies in conjunction with frictionless kinematic joints; the hypothesis of knife-edge contact between the bicycle wheels and the ground; and the simplified representation of the rider as a rigid body attached to the rear frame. The modeling limitations mentioned above can be respectively alleviated progressively by introducing structural elements in the model to represent the chas-

sis flexibility and the inclusion of friction forces in the joints (for example, dry friction); with the use of three-dimensional wheels having, for instance, toroidal geometry and considering a general representation of the wheel-ground contact by employing non-generalized coordinates (rigid body contact) or by using nonlinear finite element procedures (flexible body contact); and resorting to separate multibody modeling of the rider as a dummy body model with a basic feedback control system acting on the bicycle steering axis.

Nowadays, the possibilities of computer-aided engineering allow for the development of increasingly more precise and complex virtual models. Especially in the case of two-wheeled vehicles, and more in general for road vehicles, both modeled within the multibody computational framework, there are several open challenges and many possible directions for future research. Therefore, future research works can be focused on different interesting aspects. First, the proposed bicycle model could be used as the starting point for developing a feedback controller to stabilize the roll angular displacement of the bicycle through the use of an appropriate control torque applied to the steering mechanism. The uncontrolled bicycle shows an interesting self-stabilizing behavior strongly affected by the system geometry and its mass distribution. Therefore, many critical dynamic characteristics should be considered before including an active rider model into any bicycle model. Another interesting direction of future research could be introducing a more accurate model of the bicycle rider. To this end, for example, the implementation of a simple musculoskeletal model could be useful to understand how the motion and the loads are transmitted from the rider to the vehicle, and how these affect the overall dynamic behavior of the whole bicycle-rider system. Finally, in this work, a nonlinear set of nonholonomic constraints representing the condition of pure rolling of the wheels is employed to model the wheel-road contact. Therefore, since the physical modeling of the forces between the tire and the road significantly influences the dynamical behavior of road vehicles, future research works could also be focused on developing a more accurate description of the wheel-road interaction, including, for example, a simplified three-dimensional tire model in the bicycle multibody model developed in this paper.

To conclude, there are several fundamental issues concerning the kinematics and dynamics of two-wheeled vehicles in general, like bicycles and motorcycles, that should be addressed in future works. These are, but not limited to, the use of tire models as well as the inclusion of structural elements for modeling the system flexibility; the development of advanced systems specifically devised for improving the stability and enhance the handling of two-wheeled vehicles, such as Advanced Driver Assistance Systems (ADAS), Anti-lock Braking Systems (ABS), and Electronic Stability Control (ESC) systems; the construction of more advanced benchmark models of two-wheeled systems, such as the multibody model proposed in this paper, that allow for establishing a common reference in the research and industry communities for assessing the quality and the performance of a given design solution; the definition of a sufficiently accurate model for the rider to be able to capture the interaction of the rider-vehicle dynamics correctly; the use of modern techniques of artificial intelligence, such as the algorithms of machine learning or the deep reinforcement learning approach, for the design of effective control systems employed for solving at the same time the stabilization and the navigation problem of two-wheeled vehicles; and the implementation of the techniques used in applied system identification in conjunction with the Kalman filtering methods to construct simplified model of this family of dynamical systems for estimating physical meaningful quantities that cannot directly measured in two-wheeled vehicles, such as the roll angle and the lateral forces. These important issues will be addressed in future investigations.

Author Contributions

This research paper was principally developed by the first author (Carmine Maria Pappalardo). Great support was provided by the second author (Antonio Lettieri). The detailed review carried out by the third author (Domenico Guida) considerably improved the quality of the work. The manuscript was written through the contribution of all authors. All authors discussed the results, reviewed and approved the final version of the manuscript.

Conflict of Interest

The authors declared no potential conflicts of interest with respect to the research, authorship, and publication of this article.

Funding

The authors received no financial support for the research, authorship, and publication of this article.

References

[1] Shabana, A.A., Dynamics of multibody systems, Cambridge university press, New York, USA, 2003.
[2] Blundell, M., Harty, D., Multibody systems approach to vehicle dynamics, Elsevier, Oxford, UK, 2004.
[3] Shabana, A.A., Computational dynamics, John Wiley & Sons, London, UK, 2009.
[4] Meijaard, J.P., Papadopoulos, J.M., Ruina, A., Schwab, A.L., Linearized dynamics equations for the balance and steer of a bicycle: A benchmark and review, Proceedings of the Royal Society A: Mathematical, Physical and Engineering Sciences, 463(2084), 2007, 1955–1982.
[5] Kooijman, J.D.G., Schwab, A.L., Meijaard, J.P., Experimental validation of a model of an uncontrolled bicycle, Multibody System Dynamics, 19(1-2), 2008, 115-132.
[6] Barbagallo, R., Sequenzia, G., Cammarata, A., Oliveri, S.M., Fatuzzo, G., Redesign and multibody simulation of a motorcycle rear suspension with eccentric mechanism, International Journal on Interactive Design and Manufacturing (IJIDeM), 12(2), 2018, 517-524.
[7] Palomba, I., Richiedei, D., Trevisani, A., Two-stage approach to state and force estimation in rigid-link multibody systems, Multibody System Dynamics, 39(1-2), 2017, 115-134.
[8] Carpinelli, M., Gubitosa, M., Mundo, D., Desmet, W., Automated independent coordinates' switching for the solution of stiff DAEs with the linearly implicit Euler method, Multibody System Dynamics, 36(1), 2016, 67-85.
[9] Bruni, S., Meijaard, J.P., Rill, G., Schwab, A.L., State-of-the-art and challenges of railway and road vehicle dynamics with multibody dynamics approaches, Multibody System Dynamics, 49, 2020, 1-32.
[10] Tasora, A., Mangoni, D., Negrut, D., Serban, R., Jayakumar, P., Deformable soil with adaptive level of detail for tracked and wheeled vehicles, International Journal of Vehicle Performance, 5(1), 2019, 60-76.
[11] Soria, L., Peeters, B., Anthonis, J., Van Der Auweraer, H., Operational modal analysis and the performance assessment of vehicle suspension systems, Shock and Vibration, 19(5), 2012, 1099-1113.
[12] Popp, K., Schiehlen, W.O., Ground Vehicle Dynamics, Springer, Berlin, 2010.
[13] Wong, J.Y., Theory of Ground Vehicles, Wiley, Hoboken, 2008.
[14] Meli, E., Magheri, S., Malvezzi, M., Development and implementation of a differential elastic wheel–rail contact model for multibody applications, Vehicle system dynamics, 49(6), 2011, 969-1001.
[15] Cajic, M. S., Lazarevic, M. P., Determination of joint reactions in a rigid multibody system, two different approaches, FME Transactions, 44(2), 2016, 165-173.
[16] Vlasenko, D., Kasper, R., Generation of equations of motion in reference frame formulation for fem models, Engineering Letters, 16(4), 2008, 537-544.

[17] Geier, A., Kebbach, M., Soodmand, E., Woernle, C., Kluess, D., Bader, R., Neuro-musculoskeletal flexible multibody simulation yields a framework for efficient bone failure risk assessment, Scientific reports, 9(1), 2019, 1-15.
[18] Kebbach, M., Grawe, R., Geier, A., Winter, E., Bergschmidt, P., Kluess, D., D'Lima, D., Woernle, C., Bader, R., Effect of surgical parameters on the biomechanical behaviour of bicondylar total knee endoprostheses - A robot-assisted test method based on a musculoskeletal model, Scientific reports, 9(1), 2019, 1-11.
[19] Nitschke, M., Dorschky, E., Heinrich, D., Schlarb, H., Eskofier, B.M., Koelewijn, A.D., Van Den Bogert, A.J., Efficient trajectory optimization for curved running using a 3D musculoskeletal model with implicit dynamics, Scientific reports, 10(1), 2020, 1-12.
[20] Moore, J.K., Kooijman, J.D.G., Schwab, A.L., Hubbard, M., Rider motion identification during normal bicycling by means of principal component analysis, Multibody System Dynamics, 25(2), 2011, 225-244.
[21] Damsgaard, M., Rasmussen, J., Christensen, S.T., Surma, E., De Zee, M., Analysis of musculoskeletal systems in the AnyBody Modeling System, Simulation Modelling Practice and Theory, 14(8), 2006, 1100-1111.
[22] Whipple, F.J., The stability of the motion of a bicycle, Quarterly Journal of Pure and Applied Mathematics, 30(120), 1899, 312-348
[23] Carvallo, M.E., Theorie de mouvement du monocycle et de la bycyclette, MPublishing, 1901.
[24] Cossalter, V., Motorcycle dynamics, Second Edition, Lulu. Com, 2006.
[25] Moore, J., Hubbard, M., Parametric study of bicycle stability (P207), The engineering of sport, 7, 2008, 311-318.
[26] Moore, J.K., Human control of a bicycle, Davis, CA, University of California, Davis, 2012.
[27] Franke, G., Suhr, W., and Rieß, F., An advanced model of bicycle dynamics, European Journal of Physics, 11(2), 1990, 116.
[28] Papadopoulos, J.M., Bicycle steering dynamics and self-stability: a summary report on work in progress, Cornell Bicycle Research Project, Cornell University, NY, 1987.
[29] Meijaard, J.P., Derivation of the Linearized Equations for an Uncontrolled Bicycle, Internal report, University of Nottingham, UK, 2004, 1-19.
[30] Schwab, A.L., Meijaard, J.P., Papadopoulos, J.M., A Multibody Dynamics Benchmark on the Equations of Motion of an Uncontrolled Bicycle, EUROMECH Nonlinear Dynamics Conference, August, 2005, 7-12.
[31] Kooijman, J.D.G., Schwab, A.L., A review on bicycle and motorcycle rider control with a perspective on handling qualities, Vehicle System Dynamics, 51(11), 2013, 1722-1764.
[32] Limebeer, D.J.N., Sharp, R.S., Single track vehicle modelling and stability, IEEE Control Systems Magazine, October, 2006, 34-61.
[33] Schwab, A.L., Meijaard, J.P., A review on bicycle dynamics and rider control, Vehicle System Dynamics, 51(7), 2013, 1059-1090.
[34] Xiong, J., Wang, N., Liu, C., Stability analysis for the Whipple bicycle dynamics, Multibody System Dynamics, 48(3), 2020, 311-335.
[35] Xiong, J., Wang, N., Liu, C., Bicycle dynamics and its circular solution on a revolution surface, Acta Mechanica Sinica, 36(1), 2019, 220-233.
[36] Basu-Mandal, P., Chatterjee, A., Papadopoulos, J.M., Hands-free circular motions of a benchmark bicycle, Proceedings of the Royal Society A: Mathematical, Physical and Engineering Sciences, 463(2084), 2007, 1983-2003.
[37] Escalona, J.L., Recuero, A.M., A bicycle model for education in multibody dynamics and real-time interactive simulation, Multibody System Dynamics, 27(3), 2012, 383-402.
[38] Escalona, J.L., Kłodowski, A., Munoz, S., Validation of multibody modeling and simulation using an instrumented bicycle: from the computer to the road, Multibody System Dynamics, 43(4), 2018, 297-319.
[39] Frosali, G., Ricci, F., Kinematics of a bicycle with toroidal wheels, Communications in Applied and Industrial Mathematics, 3(1), 2012, 424.
[40] Astrom, K.J., Klein, R.E., Lennartsson, A., Bicycle dynamics and control: adapted bicycles for education and research, IEEE Control Systems Magazine, 25(4), 2005, 26-47.
[41] Plochl, M., Edelmann, J., Angrosch, B., Ott, C., On the wobble mode of a bicycle, Vehicle system dynamics, 50(3), 2012, 415-429.
[42] Tomiati, N., Colombo, A., Magnani, G., A nonlinear model of bicycle shimmy, Vehicle system dynamics, 57(3), 2019, 315-335.
[43] Schwab, A.L., Meijaard, J.P., Kooijman, J.D.G., Lateral dynamics of a bicycle with a passive rider model: stability and controllability, Vehicle system dynamics, 50(8), 2012, 1209-1224.
[44] Jansen, C., McPhee, J., Predictive dynamic simulation of Olympic track cycling standing start using direct collocation optimal control, Multibody System Dynamics, 49, 2020, 53-70.
[45] Cossalter, V., Lot, R., A motorcycle multi-body model for real time simulations based on the natural coordinates approach, Vehicle System Dynamics, 37(6), 2002, 423-447.
[46] Cossalter, V., Lot, R., Massaro, M., An advanced multibody code for handling and stability analysis of motorcycles, Meccanica, 46(5), 2011, 943-958.
[47] Sharp, R.S., Evangelou, S., Limebeer, D.J.N., Advances in the modelling of motorcycle dynamics, Multibody System Dynamics, 12(3), 2004, 251-283.
[48] Schwab, A.L., Meijaard, J.P., Papadopoulos, J.M., Benchmark results on the linearized equations of motion of an uncontrolled bicycle, Journal of mechanical science and technology, 19(1), 2005, 292-304.
[49] Wisse, M., Schwab, A.L., Skateboards, bicycles, and three-dimensional biped walking machines: Velocity-dependent stability by means of lean-to-yaw coupling, The International Journal of Robotics Research, 24(6), 2005, 417-429.
[50] Zenkov, D.V., Bloch, A.M., Marsden, J.E., The energy-momentum method for the stability of non-holonomic systems, Dynamics and Stability of Systems, 13(2), 1998, 123-165.
[51] Ruina, A., Nonholonomic stability aspects of piecewise holonomic systems, Reports on mathematical physics, 42(1-2), 1998, 91-100.
[52] Borisov, A.V., Mamayev, I.S., The dynamics of a Chaplygin sleigh, Journal of Applied Mathematics and Mechanics, 73(2), 2009, 156-161.
[53] Neimark, J.I., Fufaev, N.A., Dynamics of nonholonomic systems (Vol. 33), American Mathematical Society, USA, 2004.
[54] Pollard, B., Fedonyuk, V., Tallapragada, P., Swimming on limit cycles with nonholonomic constraints, Nonlinear Dynamics, 97(4), 2019, 2453-2468.
[55] Zhang, C., Li, Y., Qi, G., Sheng, A., Distributed finite-time control for coordinated circumnavigation with multiple non-holonomic robots, Nonlinear Dynamics, 98(1), 2019, 573-588.
[56] Pappalardo, C. M., Guida, D., On the Dynamics and Control of Underactuated Nonholonomic Mechanical Systems and Applications to Mobile Robots, Archive of Applied Mechanics, 89(4), 2019, 669-698.
[57] Sharp, R.S., On the stability and control of the bicycle, Applied mechanics reviews, 61(6), 2008, 060803.
[58] Laulusa, A., Bauchau, O.A., Review of classical approaches for constraint enforcement in multibody systems, Journal of computational and nonlinear dynamics, 3(1), 2008, 011004.
[59] Bauchau, O.A., Laulusa, A., Review of contemporary approaches for constraint enforcement in multibody systems, Journal of Computational and Nonlinear Dynamics, 3(1), 2008, 011005.
[60] Bayo, E., Ledesma, R., Augmented lagrangian and mass-orthogonal projection methods for constrained multibody dynamics, Nonlinear Dynamics, 9(1-2), 1996, 113-130.
[61] Shabana, A.A., Sany, J.R., An augmented formulation for mechanical systems with non-generalized coordinates: application to rigid body contact problems, Nonlinear dynamics, 24(2), 2001, 183-204.
[62] Pappalardo, C.M., A natural absolute coordinate formulation for the kinematic and dynamic analysis of rigid multibody systems, Nonlinear Dynamics, 81(4), 2015, 1841-1869.
[63] Pappalardo, C.M., Guida, D., A comparative study of the principal methods for the analytical formulation and the numerical solution of the equations of motion of rigid multibody systems, Archive of Applied Mechanics, 88(12), 2018, 2153-2177.
[64] Pappalardo, C.M., Lettieri, A., Guida, D., Stability analysis of rigid multibody mechanical systems with holonomic and nonholonomic constraints, Archive of Applied Mechanics, 90, 2020, 1961-2005.
[65] Pappalardo, C.M., De Simone, M.C., Guida, D., Multibody Modeling and Nonlinear Control of the Pantograph/Catenary System, Archive of Applied Mechanics, 89(8), 2019, 1589-1626.
[66] Rivera, Z.B., De Simone, M.C., Guida, D., Unmanned Ground Vehicle Modelling in Gazebo/ROS-Based Environments, Machines, 7(2), 2019, 42.
[67] De Simone, M., Rivera, Z., Guida, D., Obstacle Avoidance System for Unmanned Ground Vehicles by using Ultrasonic Sensors, Machines, 6(2), 2018, 18.
[68] De Simone, M.C., Guida, D., Control Design for an Under-Actuated UAV Model, FME Transactions, 46(4), 2018, 443-452.
[69] De Simone, M.C., Guida, D., Identification and Control of a Unmanned Ground Vehicle by using Arduino, UPB Scientific Bulletin, Series D: Mechanical Engineering, 80(1), 2018, 141-154.
[70] De Simone, M.C., Rivera, Z.B., Guida, D., Finite Element Analysis on Squeal-Noise in Railway Applications, FME Transactions, 46(1), 2018, 93-100.

ORCID iD

Carmine Maria Pappalardo https://orcid.org/0000-0003-3763-7104
Antonio Lettieri https://orcid.org/0000-0000-0000-0000
Domenico Guida https://orcid.org/0000-0002-2870-9199

How to cite this article: Carmine Maria Pappalardo, Antonio Lettieri, Domenico Guida. A General Multibody Approach for the Linear and Nonlinear Stability Analysis of Bicycle Systems. Part II: Application to the Whipple-Carvallo Bicycle Model, J. Appl. Comput. Mech., 7(2), 2021, 671-700. https://doi.org/10.22055/JACM.2020.35439.2654

Appendix A

In this appendix, for the sake of completeness, the fundamental equations of the benchmark models used for the Whipple-Carvallo bicycle system, with and without the rider, are concisely described. The numerical values of the model parameters are provided herein as well.

A.1 Benchmark Model Parameters

In the case of the benchmark bicycle model with the rider, the numerical data for the model parameters are taken from the reference [4] and are provided in Table 8.

Table 8. Benchmark bicycle model parameters.

Description	Symbol	Data (units)
Rear wheel radius	r_R	0.3 (m)
Front wheel radius	r_F	0.35 (m)
Wheelbase	w	1.02 (m)
Caster angle	λ	0.314 (rad)
Geometric trail	c	0.08 (m)
Rear frame centroid vector	$\boldsymbol{R}_B = \begin{bmatrix} x_B & 0 & z_B \end{bmatrix}^T$	$\begin{bmatrix} 0.3 & 0 & -0.9 \end{bmatrix}^T$ (m)
Front frame centroid vector	$\boldsymbol{R}_H = \begin{bmatrix} x_H & 0 & z_H \end{bmatrix}^T$	$\begin{bmatrix} 0.9 & 0 & -0.7 \end{bmatrix}^T$ (m)
Rear wheel mass	m_R	2 (kg)
Rear frame mass	m_B	85 (kg)
Front frame mass	m_H	4 (kg)
Front wheel mass	m_F	3 (kg)
Rear wheel inertia matrix	$\bar{\boldsymbol{I}}_R = \begin{bmatrix} I_{R,xx} & 0 & 0 \\ 0 & I_{R,yy} & 0 \\ 0 & 0 & I_{R,zz} \end{bmatrix}$	$\begin{bmatrix} 6.03 \cdot 10^{-2} & 0 & 0 \\ 0 & 1.2 \cdot 10^{-1} & 0 \\ 0 & 0 & 6.03 \cdot 10^{-2} \end{bmatrix}$ (kg $\times$ m^2)
Rear frame inertia matrix	$\bar{\boldsymbol{I}}_B = \begin{bmatrix} I_{B,xx} & 0 & I_{B,xz} \\ 0 & I_{B,yy} & 0 \\ I_{B,xz} & 0 & I_{B,zz} \end{bmatrix}$	$\begin{bmatrix} 9.2 & 0 & 2.4 \\ 0 & 11 & 0 \\ 2.4 & 0 & 2.8 \end{bmatrix}$ (kg $\times$ m^2)
Front frame inertia matrix	$\bar{\boldsymbol{I}}_H = \begin{bmatrix} I_{H,xx} & 0 & I_{H,xz} \\ 0 & I_{H,yy} & 0 \\ I_{H,xz} & 0 & I_{H,zz} \end{bmatrix}$	$\begin{bmatrix} 5.892 \cdot 10^{-2} & 0 & -7.56 \cdot 10^{-3} \\ 0 & 6 \cdot 10^{-2} & 0 \\ -7.56 \cdot 10^{-3} & 0 & 7.08 \cdot 10^{-3} \end{bmatrix}$ (kg $\times$ m^2)
Front wheel inertia matrix	$\bar{\boldsymbol{I}}_F = \begin{bmatrix} I_{F,xx} & 0 & 0 \\ 0 & I_{F,yy} & 0 \\ 0 & 0 & I_{F,zz} \end{bmatrix}$	$\begin{bmatrix} 1.405 \cdot 10^{-1} & 0 & 0 \\ 0 & 2.8 \cdot 10^{-1} & 0 \\ 0 & 0 & 1.405 \cdot 10^{-1} \end{bmatrix}$ (kg $\times$ m^2)

In the case of the benchmark bicycle model without the rider, the numerical data for the model parameters are taken from the reference [5] and are provided in Table 9.

In both the benchmark models, the total mass m_T of the benchmark bicycle system can be symbolically written as:

$$m_T = m_R + m_B + m_H + m_F \tag{57}$$

where m_R is the mass of the rear wheel, m_B is the mass of the rear frame, m_H is the mass of the front frame, and m_F is the mass of the front wheel. While the global coordinate y_T of the bicycle center of mass is equal to zero because of symmetry of the model,

Table 9. Benchmark riderless bicycle model parameters.

Description	Symbol	Data (units)
Rear wheel radius	r_R	0.3500 (m)
Front wheel radius	r_F	0.3485 (m)
Wheelbase	w	1.010 (m)
Caster angle	λ	0.366 (rad)
Geometric trail	c	0.190 (m)
Rear frame centroid vector	$\boldsymbol{R}_B = \begin{bmatrix} x_B & 0 & z_B \end{bmatrix}^T$	$\begin{bmatrix} 0.320 & 0 & -0.627 \end{bmatrix}^T$ (m)
Front frame centroid vector	$\boldsymbol{R}_H = \begin{bmatrix} x_H & 0 & z_H \end{bmatrix}^T$	$\begin{bmatrix} 0.907 & 0 & -0.800 \end{bmatrix}^T$ (m)
Rear wheel mass	m_R	2.56 (kg)
Rear frame mass	m_B	12.06 (kg)
Front frame mass	m_H	2.54 (kg)
Front wheel mass	m_F	2.05 (kg)
Rear wheel inertia matrix	$\bar{\boldsymbol{I}}_R = \begin{bmatrix} I_{R,xx} & 0 & 0 \\ 0 & I_{R,yy} & 0 \\ 0 & 0 & I_{R,zz} \end{bmatrix}$	$\begin{bmatrix} 7.8 \cdot 10^{-2} & 0 & 0 \\ 0 & 1.56 \cdot 10^{-1} & 0 \\ 0 & 0 & 7.8 \cdot 10^{-2} \end{bmatrix}$ (kg $\times$ m^2)
Rear frame inertia matrix	$\bar{\boldsymbol{I}}_B = \begin{bmatrix} I_{B,xx} & 0 & I_{B,xz} \\ 0 & I_{B,yy} & 0 \\ I_{B,xz} & 0 & I_{B,zz} \end{bmatrix}$	$\begin{bmatrix} 8.155 \cdot 10^{-1} & 0 & 3.27 \cdot 10^{-2} \\ 0 & 1.2 & 0 \\ 3.27 \cdot 10^{-2} & 0 & 1.0825 \end{bmatrix}$ (kg $\times$ m^2)
Front frame inertia matrix	$\bar{\boldsymbol{I}}_H = \begin{bmatrix} I_{H,xx} & 0 & I_{H,xz} \\ 0 & I_{H,yy} & 0 \\ I_{H,xz} & 0 & I_{H,zz} \end{bmatrix}$	$\begin{bmatrix} 8.60 \cdot 10^{-2} & 0 & -3.11 \cdot 10^{-2} \\ 0 & 1 \cdot 10^{-1} & 0 \\ -3.11 \cdot 10^{-2} & 0 & 1.69 \cdot 10^{-2} \end{bmatrix}$ (kg $\times$ m^2)
Front wheel inertia matrix	$\bar{\boldsymbol{I}}_F = \begin{bmatrix} I_{F,xx} & 0 & 0 \\ 0 & I_{F,yy} & 0 \\ 0 & 0 & I_{F,zz} \end{bmatrix}$	$\begin{bmatrix} 8.1 \cdot 10^{-2} & 0 & 0 \\ 0 & 1.62 \cdot 10^{-1} & 0 \\ 0 & 0 & 8.1 \cdot 10^{-2} \end{bmatrix}$ (kg $\times$ m^2)

the coordinates x_T and z_T of the bicycle centroid can be computed as:

$$\begin{cases} x_T = \frac{1}{m_T}\left(x_B m_B + x_H m_H + w m_F\right) \\ \\ z_T = \frac{1}{m_T}\left(-r_R m_R + z_B m_B + z_H m_H - r_F m_F\right) \end{cases} \tag{58}$$

where r_R and r_F denote the rear and front wheel radii respectively, w is the bicycle wheelbase, x_B and z_B represent the coordinates of the rear frame centroid, while x_H and z_H represent the coordinates of the front frame center of mass. The system mass moments of inertia $I_{T,xx}$ and $I_{T,zz}$, as well as the system product of inertia $I_{T,xz}$, computed with respect to the origin O of the global axes, are given by:

$$\begin{cases} I_{T,xx} = I_{R,xx} + I_{B,xx} + I_{H,xx} + I_{F,xx} + m_R r_R^2 + m_B z_B^2 + m_H z_H^2 + m_F r_F^2 \\ \\ I_{T,xz} = I_{B,xz} + I_{H,xz} - m_B x_B z_B - m_H x_H z_H + m_F w r_F \\ \\ I_{T,zz} = I_{R,zz} + I_{B,zz} + I_{H,zz} + I_{F,zz} + m_B x_B^2 + m_H x_H^2 + m_F w^2 \end{cases} \tag{59}$$

where $I_{R,xx}$ and $I_{R,zz}$ are the mass moments of inertia of the rear wheel, $I_{B,xx}$, $I_{B,xz}$, and $I_{B,zz}$ are the mass moments of inertia of the rear frame, $I_{H,xx}$, $I_{H,xz}$, and $I_{H,zz}$ are the mass moments of inertia of the front frame, while $I_{F,xx}$ and $I_{F,zz}$ are the mass moments of inertia of the front wheel. Note that, for all the rigid bodies, the body mass moments of inertia are defined about the centers of mass and are referred to the local frame axes that are initially aligned with the global axes. The total mass of the front assembly is denoted with m_A and is given by:

$$m_A = m_H + m_F \tag{60}$$

The coordinate y_A of the front assembly centroid is equal to zero, while the coordinates x_A and z_A of the center of mass of the front assembly can be explicitly calculated as:

$$\begin{cases} x_A = \frac{1}{m_A}\left(x_H m_H + w m_F\right) \\ \\ z_A = \frac{1}{m_A}\left(z_H m_H - r_F m_F\right) \end{cases} \tag{61}$$

The mass moments of inertia $I_{A,xx}$ and $I_{A,zz}$, as well as the product of inertia $I_{A,xz}$, computed with respect to the origin O of the global axes and related to the front assembly, are given by:

$$\begin{cases} I_{A,xx} = I_{H,xx} + I_{F,xx} + m_H\left(z_H - z_A\right)^2 + m_F\left(r_F + z_A\right)^2 \\ \\ I_{A,xz} = I_{H,xz} - m_H\left(x_H - x_A\right)\left(z_H - z_A\right) + m_F\left(w - x_A\right)\left(r_F + z_A\right) \\ \\ I_{A,zz} = I_{H,zz} + I_{F,zz} + m_H\left(x_H - x_A\right)^2 + m_F\left(w - x_A\right)^2 \end{cases} \tag{62}$$

The distance between the center of mass of the front assembly and the steering axis is indicated with u_A and can be calculated as follows:

$$u_A = (x_A - w - c)\cos(\lambda) - z_A \sin(\lambda) \tag{63}$$

where λ is the caster angle and c is the geometric trail of the bicycle benchmark model. The mass moments and products of inertia of the front assembly along the steering axis and the global axes at points where they intersect are respectively denoted with $I_{A,\lambda\lambda}$, $I_{A,\lambda x}$, and $I_{A,\lambda z}$. These quantities can be calculated as follows:

$$\begin{cases} I_{A,\lambda\lambda} = m_A u_A^2 + I_{A,xx}\sin^2(\lambda) + 2I_{A,xz}\sin(\lambda)\cos(\lambda) + I_{A,zz}\cos^2(\lambda) \\ I_{A,\lambda x} = -m_A u_A z_A + I_{A,xx}\sin(\lambda) + I_{A,xz}\cos(\lambda) \\ I_{A,\lambda z} = m_A u_A x_A + I_{A,xz}\sin(\lambda) + I_{A,zz}\cos(\lambda) \end{cases} \tag{64}$$

The bicycle geometric trail denoted with c is defined as the distance between the contact point on the front wheel and the steering axis. The mechanical trail, also known as the normal trail, is denoted as c_m and is defined as follows:

$$c_m = c\cos(\lambda) \tag{65}$$

The mechanical trail represents the distance between the intersection point, the point of intersection between the steering axis and the road, and the parallel to the steering axis, a parallel axis that is behind the steering axis and passes through the contact point. The ratio between the mechanical trail c_m and the wheelbase w is denoted with μ and is given by:

$$\mu = \frac{c_m}{w} \tag{66}$$

The gyrostatic coefficients of the rear and front wheels are respectively denoted with S_R and S_F. These coefficients are defined as follows:

$$S_R = \frac{I_{R,yy}}{r_R}, \quad S_F = \frac{I_{F,yy}}{r_F} \tag{67}$$

and

$$S_T = S_R + S_F \tag{68}$$

where S_T is the gyrostatic coefficient of both the wheels of the bicycle benchmark system. The static moment of the bicycle front assembly is denoted with S_A and can be computed as follows:

$$S_A = m_A u_A + \mu m_T x_T \tag{69}$$

The set of parameters symbolically defined here serve for the construction of the structural matrices that form the linear benchmark model of the Whipple-Carvallo bicycle system and can be numerically evaluated by using the data reported in Tables 8 and 9 to respectively determine the dynamical models with and without the presence of the rider.

A.2 Benchmark Model Equations of Motion

The equation of motion of the linear benchmark model for the Whipple-Carvallo bicycle system, with and without the rider, can be written in the following standard matrix form:

$$\boldsymbol{M}\ddot{\boldsymbol{x}} + \boldsymbol{C}\dot{\boldsymbol{x}} + \boldsymbol{K}\boldsymbol{x} = \boldsymbol{F} \tag{70}$$

where $\boldsymbol{x}$, $\dot{\boldsymbol{x}}$, and $\ddot{\boldsymbol{x}}$ respectively represent the bicycle generalized displacement, velocity, and acceleration vectors, while $\boldsymbol{K}$, $\boldsymbol{C}$, and $\boldsymbol{M}$ respectively denote the stiffness, damping, and mass matrices of the linear model, whereas $\boldsymbol{F}$ indicates the generalized external force vector applied on the bicycle benchmark model. The coordinate vector of the benchmark model denoted with $\boldsymbol{x}$ and the external force vector acting on the bicycle system denoted with $\boldsymbol{F}$ are respectively defined as follows:

$$\boldsymbol{x} = \begin{bmatrix} \phi \\ \delta \end{bmatrix}, \quad \boldsymbol{F} = \begin{bmatrix} T_\phi \\ T_\delta \end{bmatrix} \tag{71}$$

where ϕ is the rear frame roll angle, δ is the front frame steering angle, T_ϕ is the external roll torque applied between the fixed space and the rear frame, and T_δ is the external steering torque applied between the fixed space and the front frame. Using the geometrical and inertial parameters introduced in the case of the benchmark bicycle model, one can readily determine the analytical form assumed by the system mass, damping, and stiffness matrices. The mass matrix of the benchmark model denoted with $\boldsymbol{M}$ is defined as follows:

$$\boldsymbol{M} = \begin{bmatrix} M_{\phi,\phi} & M_{\phi,\delta} \\ M_{\delta,\phi} & M_{\delta,\delta} \end{bmatrix} \tag{72}$$

where the entries of the mass matrix can be explicitly determined as:

$$\begin{cases} M_{\phi,\phi} = I_{T,xx} \\ M_{\phi,\delta} = I_{A,\lambda x} + \mu I_{T,xz} \\ M_{\delta,\phi} = M_{\phi,\delta} \\ M_{\delta,\delta} = I_{A,\lambda\lambda} + 2\mu I_{A,\lambda z} + \mu^2 I_{T,zz} \end{cases} \tag{73}$$

The damping matrix of the benchmark model denoted with $\boldsymbol{C}$ can be explicitly written as:

$$\boldsymbol{C} = v\boldsymbol{C}_1 \tag{74}$$

where v is the forward velocity of the bicycle system and the matrix $\boldsymbol{C}_1$ is defined as follows:

$$\boldsymbol{C}_1 = \begin{bmatrix} C^1_{\phi,\phi} & C^1_{\phi,\delta} \\ C^1_{\delta,\phi} & C^1_{\delta,\delta} \end{bmatrix} \tag{75}$$

where the entries of the matrix $\boldsymbol{C}_1$ can be computed as reported below:

$$\begin{cases} C^1_{\phi,\phi} = 0 \\ C^1_{\phi,\delta} = \mu S_T + S_F \cos(\lambda) + \frac{I_{T,xz}}{w} \cos(\lambda) - \mu m_T z_T \\ C^1_{\delta,\phi} = -\left(\mu S_T + S_F \cos(\lambda)\right) \\ C^1_{\delta,\delta} = \frac{I_{A,\lambda z}}{w} \cos(\lambda) + \mu \left(S_A + \frac{I_{T,zz}}{w} \cos(\lambda)\right) \end{cases} \tag{76}$$

The stiffness matrix of the benchmark model denoted with $\boldsymbol{K}$ can be explicitly written as:

$$\boldsymbol{K} = \boldsymbol{K}_0 + v^2 \boldsymbol{K}_2 \tag{77}$$

where v is the longitudinal velocity of the bicycle system, the matrix $\boldsymbol{K}_0$ is a gravity-dependent matrix, and the matrix $\boldsymbol{K}_2$ is a velocity-dependent matrix. The gravity-dependent matrix denoted with $\boldsymbol{K}_0$ is defined as follows:

$$\boldsymbol{K}_0 = \begin{bmatrix} K^0_{\phi,\phi} & K^0_{\phi,\delta} \\ K^0_{\delta,\phi} & K^0_{\delta,\delta} \end{bmatrix} \tag{78}$$

where the entries of the matrix $\boldsymbol{K}_0$ can be computed as reported below:

$$\begin{cases} K^0_{\phi,\phi} = m_T z_T \\ K^0_{\phi,\delta} = -S_A \\ K^0_{\delta,\phi} = K^0_{\phi,\delta} \\ K^0_{\delta,\delta} = -S_A \sin(\lambda) \end{cases} \tag{79}$$

The velocity-dependent matrix denoted with $\boldsymbol{K}_2$ is defined as follows:

$$\boldsymbol{K}_2 = \begin{bmatrix} K^2_{\phi,\phi} & K^2_{\phi,\delta} \\ K^2_{\delta,\phi} & K^2_{\delta,\delta} \end{bmatrix} \tag{80}$$

where the entries of the matrix $\boldsymbol{K}_2$ can be computed as reported below:

$$\begin{cases} K^2_{\phi,\phi} = 0 \\ K^2_{\phi,\delta} = \frac{S_T - m_T z_T}{w} \cos(\lambda) \\ K^2_{\delta,\phi} = 0 \\ K^2_{\delta,\delta} = \frac{S_A + S_F \sin(\lambda)}{w} \cos(\lambda) \end{cases} \tag{81}$$

Once the mass, damping, and stiffness matrices of the linear benchmark model of the Whipple-Carvallo bicycle system are determined, a standard eigenvalue problem can be readily formulated and solved to trace the stability diagram associated with this mechanical system as a function of the bicycle forward velocity. Furthermore, as discussed in the paper, this dynamical model can also be used to perform a transient analysis in the presence of imposed disturbances from the configuration of dynamic equilibrium and/or externally applied torques.